Inter-membrane association of the Sec and BAM translocons for bacterial outer-membrane biogenesis

Sara Alvira[1*], Daniel W. Watkins[1*], Lucy Troman[1], William J. Allen[1], James Lorriman[1], Gianluca Degliesposti[2], Eli J. Cohen[3], Morgan Beeby[3], Bertram Daum[4], Vicki A.M. Gold[4], J. Mark Skehel[2] and Ian Collinson[1†]

[1], *School of Biochemistry, University of Bristol, BS8 1TD, United Kingdom*

[2], *Biological Mass Spectrometry and Proteomics, MRC Laboratory of Molecular Biology, Francis Crick Avenue, Cambridge, CB2 0QH, United Kingdom*

[3], *Faculty of Natural Sciences, Department of Life Sciences, Imperial College, London SW7 2AZ, United Kingdom*

[4], *Living Systems Institute, University of Exeter, EX4 4QD, United Kingdom*

[*], these authors contributed equally to this work

[†], corresponding author: ian.collinson@bristol.ac.uk

SUMMARY

The outer-membrane of Gram-negative bacteria is critical for surface adhesion, pathogenicity, antibiotic resistance and survival. The major constituent – hydrophobic β-barrel Outer-Membrane Proteins (OMPs) – are first secreted across the inner-membrane through the Sec-translocon for delivery to periplasmic chaperones *e.g.* SurA, which prevent aggregation. OMPs are then offloaded to the β-Barrel Assembly Machinery (BAM) in the outer-membrane for insertion and folding. We show the Holo-TransLocon (HTL) – an assembly of the protein-channel core-complex SecYEG, the ancillary sub-complex SecDF, and the membrane 'insertase' YidC – contacts BAM through periplasmic domains of SecDF and YidC, ensuring efficient OMP maturation. Furthermore, the proton-motive-force (PMF) across the inner-membrane acts at distinct stages of protein secretion: (1) SecA-driven translocation through SecYEG; and (2) communication of conformational changes *via* SecDF across the periplasm to BAM. The latter presumably drives efficient passage of OMPs. These interactions provide insights of inter-membrane organisation and communication, the importance of which is becoming increasingly apparent.

INTRODUCTION

Outer-membrane biogenesis in Gram-negative bacteria (reviewed in [1]) requires substantial quantities of protein to be exported; a process which begins by transport across the inner plasma membrane. Precursors of β-barrel Outer-Membrane Proteins (OMPs) with cleavable N-terminal signal-sequences are targeted to the ubiquitous Sec-machinery and driven into the periplasm by the ATPase SecA and the trans-membrane proton-motive-force (PMF) [2–5]. Upon completion, the pre-protein signal-sequence is proteolytically cleaved [6,7] , releasing the mature unfolded protein into the periplasm. The emergent protein is then picked up by periplasmic chaperones, such as SurA and Skp, which prevent aggregation [8,9], and somehow facilitate delivery to the β-Barrel Assembly Machinery (BAM) for outer-membrane insertion and folding [10,11].

In *E. coli,* BAM consists of a membrane protein complex of subunits BamA-E, of known structure [12–14]. The core component, BamA, is a 16 stranded β-barrel integral membrane protein, which projects a large periplasmic stretch of 5 POlypeptide TRanslocation-Associated (POTRA) domains into the periplasm. BamB-E are peripheral membrane lipoproteins anchored to the inner leaflet of the OM. In spite of the structural insights, the mechanism for BAM-facilitated OMP insertion is unknown [15].

The bacterial periplasm is a challenging environment for unfolded proteins, so complexes spanning both membranes are critical for efficient delivery through many specialised secretion systems [16]. How do enormous quantities of proteins entering the periplasm *via* the general secretory pathway (Sec) efficiently find their way through the cell envelope to the outer-membrane? From where is the energy derived to facilitate these trafficking processes some distance from the energy transducing inner-membrane, and in an environment lacking ATP? Could it be achieved by a direct interaction between chaperones, and the translocons of the inner (Sec) and outer (BAM) membranes?

The core-translocon, SecYEG, does not possess periplasmic domains of sufficient size to mediate such an interaction [17]. However, the Holo-TransLocon (HTL) contains the ancillary sub-complex SecDF and the membrane protein ‘insertase’ YidC [18,19], both of which contain periplasmic extensions potentially large enough to reach the POTRA domains of BamA.

SecDF is a member of the so called Root Nodulation Division (RND) superfamily of PMF-driven transporters (reviewed in [20]). It is a highly conserved component of the bacterial Sec

translocon, wherein it has long been known to facilitate protein secretion [18,21,22]. While fellow component of the HTL – YidC – is essential for membrane protein insertion, and thus indispensable [23,24]. Mutants of *secD* and *secF* are not fatal, but severely compromised and cold-sensitive [25]; presumably due to deficiencies in envelope biogenesis. The cause of this has been ascribed to a defect in protein transport across the inner membrane.

In keeping with other members of the RND family, like AcrB [26], SecDF confers PMF stimulation of protein secretion [27]. Different structures of SecDF show the large periplasmic domains in different conformational states [28–30], also affected by altering a key residue of the proton transport pathway ($SecD_{D519N}$ – *E. coli* numbering) [28]. On this basis, an elaborate mechanism has been proposed whereby PMF driven conformational changes, at the outer surface of the inner-membrane, pick up and pull polypeptides as they emerge from the protein-channel exit site of SecY. Yet, ATP- and PMF-driven translocation across the inner membrane does not require SecDF or YidC; SecYEG and SecA will suffice [2,19]. Evidently then, there must be two PMF-dependent components of protein secretion: one early stage dependent only on SecYEG/ SecA, and another later event regulated by an AcrB-like SecDF activity. This distinction has not been fully appreciated.

This study explores the role of the ancillary components of the Sec machinery for protein secretion and downstream trafficking through the periplasm; for delivery to the outer-membrane and OMP maturation. In particular, we examine the possibility of a direct interaction between the HTL and BAM machineries to facilitate protein transport through the envelope. The basic properties and structure of the inter-membrane super-complex are investigated, as well as its importance for OMP folding and insertion. The implications of this interaction and its modulation caused by proton transport through SecDF are profound. Thus, we consider their consequences for the mechanism of protein transport through the Sec and BAM machineries, and for outer-membrane biogenesis.

RESULTS

Co-fractionation and immunoprecipitation highlight an interaction between the Sec and BAM machineries

Total *E. coli* membranes from cells over-producing either SecYEG or HTL were prepared and fractionated by sucrose gradient centrifugation to separate the inner- and outer-membranes (Figure 1a). We first sought to determine the precise locations of the respective inner- and outer-membrane proteins in the fractions; SDS-PAGE analysis of the fractions stained for total protein revealed the presence of SecY in the lighter inner-membrane fractions (Figure 1 –figure supplement 1a, yellow asterisk – left panel). Heating the fractions (required to unfold outer membrane proteins) prior to SDS-PAGE helped reveal the location of the most highly expressed outer membrane residents (OmpC and OmpF; Figure 1 –figure supplement 1a, yellow asterisk – right panel). Thus, in these gradients fractions 1-2 mostly contain outer-membranes, and fractions 4-5 are composed mainly of inner-membranes.

Immunoblotting confirmed the presence of the BAM components (BamA, BamB and BamD), as expected, in outer-membrane fractions (OM; Figure 1b). Likewise, the over-produced SecY and SecE subunits mark the fractions containing the core-complex (SecYEG) in the inner-membrane fractions (IM; Figure 1b, YEG↑). However, when over-produced as part of HTL there is a marked shift of their migration peak towards the outer-membrane containing fractions (Figure 1b, HTL↑). Interestingly, the over-production of SecDF alone results in a similar effect (Figure 1c); where SecD, SecY and SecG all migrate into the outer-membrane containing fractions. An effect which was lost in comparable experiments where the periplasmic domain of SecD (P1) had been removed (Figure 1c). Our interpretation of these experiments is that the interaction between the Sec and Bam complexes, requiring at least the periplasmic domains of SecD (and most likely SecF and YidC), causes an association of inner and outer membrane vesicles reflected in the shift we observe.

To further examine this interaction, we extracted native membranes with a mild detergent for Immuno-Precipitation (IP) using a monoclonal antibody raised against SecG. The pull-downs were then probed for native interacting partners by western blotting (Figure 1d,e; Figure 1 –figure supplement 1b). As expected, SecG (positive control) and SecD of HTL co-immuno-precipitated. Crucially, BamA could also be detected. The specificity of the association was demonstrated by controls omitting the SecG antibody or the SecG protein (produced from membranes extracts of a *ΔsecG* strain [31]), wherein non-specific binding was either undetectable, or considerably lower than the specific co-immuno-precipitant (Figure 1d). When

BAM was over-produced, the yield of BamA recovered in the IPs increased accordingly (Figure 1d,e; Figure 1 –figure supplement 1b).

In a similar experiment, a hexa-histidine tagged BamA was used to isolate BAM from cells over-producing the complex. Western blots showed that BamA co-purified, as expected, with additional components of the BAM complex (BamB and BamD), and crucially also with SecD and SecG of the HTL (Figure 1f; Figure 1 –figure supplement 1c). Again, controls (omitting Ni^{2+}, or recombinant his_6-BamA) were reassuringly negative.

Interaction between HTL and BAM is cardiolipin dependent

The phospholipid CardioLipin (CL) is known to be intimately associated with energy transducing systems, including the Sec-machinery, for both complex stabilisation and efficient transport [19,32,33]. For this reason, the IP experiments above were augmented with CL. On omission of CL the interactions of SecG with SecD and BamA were reduced ~ 3- and 5-fold, respectively (Figure 1d,e; Figure 1 –figure supplement 1b). This lipid-mediated enhancement of the SecG-SecD interaction is consistent with our previous finding that CL stabilises HTL [19], and shows it also holds true for the HTL-BAM interaction. *Apropos*, CL has been shown to be associated with the BAM complex [34].

HTL and BAM interact to form an assembly large enough to bridge the inner- and outer-membranes

To confirm the interaction between the Sec and BAM machineries, the purified complexes were subjected to glycerol gradient centrifugation. When mixed together, HTL and BAM co-migrated towards higher glycerol concentrations, beyond those attained by the individual complexes (Figure 2a, yellow asterisk) and consistent with the formation of a larger complex due to an interaction between the two. The interaction is clear, but not very strong; only a fraction of the HTL and BAM associate. This is likely due to the required transient nature of the association between the two translocons *in vivo*, and also because of the complete breakdown of the inner- and outer-membranes by detergent – required for this experiment. When the experiment was repeated with the individual constituents of HTL: SecDF and YidC, but not SecYEG, were also shown to interact with BAM (Figure 2 –figure supplement 1 a-c,

yellow asterisks). Again, the incomplete association suggest their affinity for one another is not high.

Visualisation of the heavy fractions containing interacting HTL and BAM by Negative Stain Electron Microscopy (EM) revealed a heterogeneous mixture of small and very large complexes (Figure 2 –figure supplement 2a, large complexes marked with white arrows). As noted above, this mixed population is probably due to the expected transient nature of the interaction between the two complexes, and/ or due to super-complex instability caused by loss of the bilayer and specifically bound phospholipids, *e.g.* CL, during purification (see above and below). Even though we augment the material with CL, it is unlikely the full complement of lipids found in the native membrane bound state are restored.

To overcome this heterogeneity we stabilised the complex by cross-linking, using GraFix [35] (Figure 2 –figure supplement 3a, left). Note that successful stabilisation of the assembly by cross-linking was also demonstrated by size exclusion chromatography – performed for sample preparation for cross-linked mass spectrometry (XL-MS) and cryo-EM (see next section). We confirmed the presence of BAM and HTL constituents in the cross-linked fraction by mass spectrometry (Figure 2 –figure supplement 3a, right, Figure 2 –source data 1) and subsequently analysed it by negative stain EM, which revealed a marked reduction in the number of dissociated complexes (Figure 2 –figure supplement 2b). As expected, omitting CL from the preparation results in dissociation of the majority of the large complexes, even with GraFix (Figure 2 –figure supplement 2c), supporting the above findings regarding CL dependence of the interaction (Figure 1e).

The subsequent single particle analysis of the cross-linked material (Figure 2 –figure supplement 3a, left, black asterisk; Figure 2 –source data 2) revealed a remarkable structure large enough (~ 300 x 250 x 150 Å) to contain both Sec and BAM machineries [14,36], and with a height sufficient to straddle the space between the two membranes (Figure 2b; Figure 2 –figure supplement 3b), especially when considering the plasticity of the periplasm [37]. Moreover, the periplasmic domains of the HTL and BAM complexes are potentially large enough reach out across the space between the inner- and outer-membranes to contact one another. Indeed, regions of SecDF and the POTRA domains of BamA have been show to extend ~ 60 Å [28] and ~ 110 Å [38] respectively, sufficient to bridge this gap.

To assign the locations and orientations of the individual constituents of HTL and BAM, we compared the 3D reconstructions of different sub-complexes: BAM bound to SecYEG-DF (without YidC) (Figure 2 –figure supplement 3c) or SecDF alone (Figure 2 –figure supplement 3d). The difference analysis revealed the locations of YidC (Figure 2b, pink; Figure 2 –figure supplement 3c, pink arrow), SecDF (Figure 2b, green; Figure 2 –figure supplement 3d, green arrow) and SecYEG (Figure 2b, blue; Figure 2 –figure supplement 3d, blue arrow) at the bottom of the assembly (assigned as the inner-membrane region). The orientation of BAM relative to SecDF is different in SecDF-BAM compared to HTL-BAM (Figure 2 –figure supplement 3d, red arrows), possibly due to its known ability to move (see below), and/ or the absence of stabilising interactions with the missing HTL components (SecYEG and YidC).

Removing BamB from the complex results in the loss of significant mass in the area designated as the outer-membrane region (Figure 2b, orange; Figure 2 –figure supplement 3e, orange arrow). This confirmed the orientation of the respective inner- and outer-membrane associated regions, and the assignment of the BAM complex as shown in Figure 2b. Interestingly, the complex lacking BamB shows a diminishment of the density assigned as YidC (Figure 2 –figure supplement 3e, pink arrow), suggestive of a mutual interaction between the two.

Periplasmic domains of the Sec and BAM translocons associate to form a large cavity between the bacterial inner- and outer-membranes

Despite heterogeneity in the sample we were able to isolate a cross-linked HTL-BAM complex by size exclusion chromatography and produce a low-resolution cryo-EM structure (Figure 2c; Figure 2 –figure supplement 4; Figure 2 –figure supplement 5a (a similar fraction was used to that marked by the black asterisk) and Figure 2 –source data 2) with an overall resolution of 18.23 Å. Taken together with the difference map generated by negative stain-EM (Figure 2b; Figure 2 –figure supplement 3) the structure reveals the basic architecture of the assembly and the arrangement of constituent subunits.

The complexity of the image processing resulted in an insuffient number of particles of a single class to attain high-resolution. Many factors contribute to this problem: the dynamism of the complex, due to the limited contact surface between the HTL and BAM; its inherent mobility necessary for function; the presence of detergent surrounding the trans-membrane

regions of the HTL and BAM components, accounting for most of the surface of the assembly; and finally, the absence of inner- and outer-membrane scaffolds. The loss of the fixed double membrane architecture was particularly problematic; during image processing we found different sub-populations where BAM pivots away from its raised position towards where the inner membrane would otherwise have been. Obviously, this would not happen if restrained by the outer-membrane.

In spite of all this, the attainable structure proved to be very illuminating. Due to the limited resolution, we deployed cross-linking mass spectroscopy (XL-MS) to verify the contacts between HTL and BAM responsible for inter-membrane contact points. The HTL and BAM complexes were mixed together in equimolar quantities and cross-linked with the lysine-specific reagent DSBU. The reaction mixture was then fractionated by gel filtration chromatography and analysed by SDS-PAGE. A single band corresponding to the cross-linked HTL-BAM complex was detected (Figure 2 –figure supplement 5a, lower band, black asterisk); note that the isolation of the intact HTL-BAM complex by size exclusion chromatography provides further evidence of a genuine interaction between inner- and outer-membrane translocons. The fraction containing the cross-linked complex was combined and digested prior to LC-MS/ MS analysis.

The analysis of mass spectrometry data enabled the detection and mapping of the inter- and intra-molecular protein cross-links within the assembly. The results show an intricate network of interactions most of which are consistent with the cryo-EM structure, particularly at one side of the assembly between SecD and BamBCD, and on the other side between YidC and BamABCD (Figure 2 –figure supplement 5b,c).

All the constituent proteins of HTL were cross-linked to BAM subunits with the exception of SecG and YajC. Thus, the co-immunoprecipitation and affinity pull down of SecG together with BamA (described above; Figure 1d-f) must have been the result of an indirect interaction, presumably bridged *via* SecDF-YidC, which interacts with both SecG and BAM. This is consistent with the lack of an interaction of SecYEG alone with the BAM complex (Figure 2 – figure supplement 1a), and the assignment of the electron microscopy structures (Figure 2b,c) – also showing no connection between SecYEG and BAM. In this respect, it is interesting to note in the structure that the periplasmic domains of SecD, YidC and to a lesser degree SecF, extend to establish multiple interactions with the BAM lipoproteins suggesting a pivotal role

for these subunits in the formation of the HTL-BAM complex (Figure 2c,d). This bridge between the two complexes also helps to define a very large cavity between the inner- and outer-membrane regions (Figure 2d).

The BAM complex is recognisable in the cryo-EM structure at the outer membrane with the expected extensive periplasmic protrusions [12,13]. Some components of the BAM complex, such as BamB, can be unambiguoulsy docked into the cryo-EM structure (Figure 2c), localised by negative stain difference mapping (Figure 2b and Figure 2 –figure supplement 3e), and its recognisable β-propeller shape [12,13]. We also suggest the locations of BamA, BamC and BamD according to the cryo-EM density and the constraints of the XL-MS data (Figure 2e; Figure 2 –figure supplement 5c).

The inner-membrane region of the HTL – while bound to BAM – is much more open than the previous structure of the isolated version [36]. In the new open structure, the locations of the core-complex SecYEG, SecDF and YidC can be easily distinguished; the former two being connected within the membrane by two bridges (Figure 2f, left). These connections could be the binding sites of CL and the central lipid pool identified previously, required for structural stability and translocon activity [19,32,39]. Within SecYEG the protein-channel can be visualised though the centre, along with the lateral gate (required for signal sequence binding and inner membrane protein insertion) facing towards SecDF, YidC and the putative central lipid pool [39](Figure 2f, right).

Cardiolipin, required for super-complex formation, stabilises an 'open' form of the HTL

As mentioned above, the HTL bound to BAM in our EM structure (Figure 3a, structure ii) seems to be more open when compared to the previously published low-resolution cryo-EM structure [36] (emd3056; Figure 3a, structure i), and also displays a more prominent periplasmic region. Preparations of HTL alone, made in this study, contain both a 'compact' state (Figure 3a, structure iii) similar to that of the previously published structure (Figure 3a, structure i), as well as a proportion of an 'open' state, with proud periplasmic domains, not previously described (Figure 3a, structure iv), and apparently more similar to that seen in the HTL-BAM structure (Figure 3a, structure ii).

The HTL sample used here is extremely pure, of known subunit composition and not prone to oligomerisation [19]. So, we can rule out that this larger form, assigned as an 'open' state, of

HTL is not due to the presence of contaminants, unknown additional partner proteins, or dimerisation. Lipid content within the HTL is critical for proper structure and function, and CL is particularly important for protein translocation through the Sec machinery [19,32,33,40]. Depletion of these core lipids, for instance by detergent extraction, might be expected to cause a collapse of the complex. Therefore, the reason for the presence of these different populations of the HTL – 'compact' and 'open' states – is likely due to varying interactions with lipids, including CL. In line with this hypothesis, augmenting the HTL with CL during purification increased the proportion of the 'open' state (from 8% to 17%), which could be enriched by glycerol gradient fractionation (to 32%), and further stabilised by cross-linking (to 40%) (Figure 3 –figure supplement 1).

Evidently then, it seems likely that the open conformation (Figure 3a, structure iv) is the state capable of interacting with the BAM complex (Figure 3a, structure ii). The 'open' structure, and the 'compact' structure seen before [36], may reflect different functional states of the translocon. Presumably, the HTL would be closed when idle in the membrane, and would open to various degrees depending on the associated cytosolic partners (*e.g.* ribosomes or SecA), periplasmic factors (chaperones, BAM, *etc*.) and various substrates (*e.g.* globular, membrane or β-barrels). Thus, it is not suprising that when free of the constraints of the membrane, and in the harsh environment of a detergent micelle, that these various states can be adopted – explaining the observed heterogeneity.

Increasing the distance between inner- and outer-membranes weakens the HTL-BAM interaction

The dimensions of the HTL-BAM structure roughly correspond to the distance between the inner- and outer-membranes, but only just. Thus, increasing the thickness of the periplasm might therefore be expected to stymie formation of HTL-BAM complexes, as previously observed for other trans-periplasmic complexes [41,42]. To test this prediction, we increased the thickness of the periplasm by manipulating the width-determining lipoprotein Lpp, which separates the outer-membrane from the peptidoglycan layer. Increasing the length of *lpp* thus increases the width of the periplasm, from ~ 250 Å for wild-type *lpp* to ~ 290 Å when an additional 21 residues are added to the resultant protein (Lpp^{+21}) [41] (Figure 4a).

The experiments described above (Figure 1d,e) were repeated: extracting total membranes in the presence of CL for IP by antibodies raised against SecG. Blotting for SecD and BamA then provided a measure respectively for interactions within HTL, and between HTL and BAM (Figure 4b,c; Figure 4 –figure supplement 1) in the *lpp*$_{+21}$ genetic background. Consistent with our model, when the inter-membrane distance was increased, the integrity of the HTL in the inner membrane was unaffected, but the recovery of HTL-BAM was reduced more than 3-fold (Figure 4b,c; Figure 4 –figure supplement 1).

PMF stimulation of protein translocation through the inner membrane by SecA and SecYEG is not conferred by proton passage through SecD

It has been known for many years that SecDF plays a critical role in protein secretion. The results above show that the periplasmic domains of HTL, and in particular those of SecDF, mediate the recruitment of the BAM complex, likely to facilitate the onward journey of proteins to the outer membrane. Therefore, we decided to re-evaluate the precise role and activity of this ancillary sub-complex. Experiments were established to investigate: (1) the role of SecDF in SecA dependent protein transport through the inner membrane *via* SecYEG, and (2) the consequences of its interaction with the BAM machinery for outer-membrane protein maturation. In particular, we set out to explore the possibility of an active role in these events for the proton translocating activity of the SecDF sub-complex.

secDF null mutants exhibit a severe export defect, and are only just viable [22]. To explore this phenotype further we utilised *E. coli* strain JP325, wherein the expression of *secDF* is under the control of an *ara* promoter: the presence of arabinose or glucose, respectively results in production or depletion of SecDF-YajC [21] (Figure 5a; Figure 5 –figure supplement 1a). To begin with, we grew cultures of JP325 containing either an empty vector, recombinant *secDF* or *secD*$_{D519N}$*F* overnight in permissive (0.2% arabinose) conditions. The following morning excess arabinose was washed away by centrifugation and resuspension, before applying to plates containing either arabinose or glucose, for continued production or depletion of endogenous SecDF-YajC, respectively.

Depletion of SecDF-YajC results in a strong growth defect (Figure 5b, panels 1 and 2), which can be rescued by recombinant expression of *wild type secDF* [43] (Figure 5b, panels 3 and 4). In contrast, expression of *secD*$_{D519N}$*F*, which results in the production of a complex incapable

of proton transport [28], did not complement the defect (Figure 5b, panels 5 and 6). This phenotype is consistent with a general secretion defect, shown previously [25].

In order to determine if this secretion defect is due to a problem in translocation through the inner membrane (HTL), or beyond, we set up a classical *in vitro* transport assay: investigating SecA-driven proOmpA transport into inner membrane vesicles (IMVs) containing either over-produced native HTL, or the defective version of HTL (containing $SecD_{D519N}F$). Both sets of vesicles contained similar concentrations of SecY (Figure 5 –figure supplement 1b), yet despite the blocked proton pathway through SecDF, there was little difference in the efficiencies of transport (Figure 5c). The lower quantities of transported pre-protein compared to experiments conducted with IMVs made from cells over-producing only the core-complex (SecYEG), seen also previously [19], most likely reflects the reduced quantities of SecYEG in the IMVs made from HTL producing cells, measured by blotting for SecY (Figure 5 –figure supplement 1b).

Most importantly, the results demonstrate that SecA mediated ATP and PMF driven protein translocation through the inner membrane *via* HTL does not require a functional proton wire through SecDF (Figure 5c). In this respect, SecYEG and SecA are sufficient [2]. Therefore, the proton translocating activity of SecD, needed for general secretion and cell survival, must be required for something downstream of protein transport through the inner membrane.

Interaction between the Sec and BAM complexes is required for efficient OmpA folding

The most obvious function of an interaction between the Sec and BAM machineries would be to facilitate efficient delivery and insertion of OMPs to the outer-membrane. We therefore reasoned that disrupting this interaction might compromise OMP delivery to BAM, leading to the accumulation of unfolded OMPs in the periplasm – particularly when high levels of outer-membrane biogenesis are required, such as in rapidly dividing cells.

Elevated levels of unfolded OmpA (ufOmpA) in the periplasm are a classical signature of OMP maturation deficiencies [9,44]. It can be easily monitored by SDS-PAGE and western blotting: folded OmpA (fOmpA) does not denature fully in SDS unless boiled; it therefore runs at a lower apparent molecular mass compared to ufOmpA when analysed by SDS-PAGE (Figure 5d, left; Figure 5 –figure supplement 1c) [9,44]. Importantly, we confirm the distinct identities of ufOmpA and fOmpA bands in the western blots by the analysis of native (folded) and boiled OmpA (unfolded). We also show the unfold and folded forms also migrate

differently from the precursor – proOmpA (Figure 5 –figure supplement 1c). Therefore, the subsequent periplasmic analysis could not have been confused by un-secreted pre-protein – potentially from contaminating cytosol.

Based on the above results, SecDF looks like the most important mediator of the Sec-BAM interaction. We therefore used the SecDF depletion strain (JP325) as a basis for functional assays. To overcome the growth defect (Figure 5b, panels 1 and 2) and produce sufficient cells to analyse, overnight cultures of the strains used above were grown in permissive media (arabinose). Cells were then washed thoroughly to remove arabinose and transferred to new media containing glucose (non-permissive), or maintained in arabinose as a control, then resuspended to give an OD_{600nm} = 0.05 (marked as t = 0 in Figure 5a, d, e-g). Samples were taken from the growing cultures at regular intervals and the ratio of unfolded to folded OmpA determined (Figure 5d, g), along with cell density (Figure 5f) and SecD levels (Figure 5e). Under SecDF depletion conditions (red squares), high levels of unfolded OmpA accumulate in the periplasm, particularly during the exponential phase when the demand for outer-membrane biogenesis is highest (Figure 5d, yellow asterisk; Figure 5f,g; Figure 5 –figure supplement 1d). Meanwhile, under permissive conditions (Figure 5e-g, arabinose, orange circles), a more modest increase in ufOmpA is observable after 1.5 h, but it recovers fully by 3 h. Notably, this change is accompanied by a transient decrease in SecDF levels (Figure 5e, orange circles).

We know that these experiments were not compromised by the precursor proOmpA, which was not present in the periplasmic samples (Figure 5 –figure supplement 1c). However, in some cases a spurious band appeared in the OmpA western blots, between the unfolded and folded forms (Figure 5 –figure supplement 1c, red asterisk; Figure 5 –figure supplement 1d). The band was only apparent in samples derived from overnight cultures grown in the presence of arabinose, including in the *wild type* parent strain MC4100 (Figure 5 –figure supplement 1c, far right lane, red asterisk). The stationary state of these cultures, grown in permissive and native conditions – with no impediment, or high demand for OmpA maturation – should not induce a build up of unfolded OmpA. So, it is unlikely that this spurious band represents an additional unfolded state of OmpA, and was ignored in the analysis.

Clearly, the expression of *secDF* and levels of ufOmpA in the cell envelope are anti-correlated, exacerbated during fast cell growth. These effects were not an indirect consequence of BamA loss, which was unperturbed (Figure 5 –figure supplement 1e). Taken together, the

data show that depletion of SecDF reduces the interaction between HTL and BAM, and thereby hampers transport of β-barrel proteins to the outer-membrane – resulting in a build-up of ufOmpA in the periplasm. A backlog of unfolded OMP could compromise outer membrane biogenesis and its integrity, and thereby explain the cold-sensitivity of *secDF* mutants [25]. This seems the most plausible explanation as transport through the inner membrane is uaffected by the absence of SecDF [19] (Figure 5c).

Proton transport through SecD is required for efficient outer membrane protein maturation

Proton translocation through SecD is crucial for cell growth (Figure 5b, panels 5 and 6), but evidently not for PMF-stimulated protein transport through the inner membrane *via* SecYEG (Figure 5c). To determine if this activity is required for downstream events – such as delivery of OMP to the outer-membrane – we once again deployed the SecDF depletion strain, complemented with wild-type or mutant *secDF* (as above, Figure 5b, panels 3 - 6), wherein the mutant produced SecD incapable of proton transport ($SecD_{D519N}$).

Comparable quantities of the respective SecD variants could be produced (Figure 5e, green and purple; Figure 5 –figure supplement 1a). The subsequent analysis showed the wild type, but not the mutant, reduced unfolded OmpA in the periplasm to levels much closer to that of the strain grown in permissive conditions (Figure 5g; green and purple, respectively; Figure 5 –figure supplement 1d). Therefore, proton transport through SecD is apparently required for efficient outer-membrane protein folding.

To confirm the defective variant $SecD_{D519N}F$ still interacts with BAM, we repeated co-IP experiments as before (Figure 1d, e) using membrane extracts derived from the SecDF depletion strains grown in the non-permissive condition (glucose; Figure 5b), but complemented with plasmids driving the expression of the *wild type* or mutant *secDF*, or nothing at all (empty plasmid). Again, in order to prepare sufficient material, overnight cultures were grown in media containing arabinose, and then transferred to new media containing glucose. At OD_{600nm} = 1.0, the cultures were harvested and membranes were prepared and solubilised for IP with SecG antibodies (Figure 5h,i; Figure 5 –figure supplement 1f,g). As expected the immuno-precipitated yields of SecG were invariant, but the depletion of SecD (cells harbouring only the empty vector; Figure 5 –figure supplement 1g) reduced the recovery of BamA commensurately

(Figure 5h,i). The levels of co-immuno-precipitated SecG, SecD and BamA were the same irrespective of complementation with the *wild type* or mutant forms of *secDF*. Evidently then, the intergrity of the HTL and its ability to interact with the BAM complex do not require a functional proton wire through SecD. Therefore, the mutant's compromised OmpA maturation must be due to the loss of proton flow through SecD, rather than a loss of contact between HTL and BAM.

HTL(SecD$_{D519N}$F) adopts a different conformation to the native version

The PMF-dependent mobility of the periplasmic domain of SecD [28] seems like it might be critical for its activity as part of the BAM-HTL complex. To test this, the variant of HTL containing SecD$_{D519N}$ was produced for comparison with the native form. Electron microscopy was used to assess the extent of 'compact' and 'open' forms of the HTL complex (Figure 3; Figure 6, respectively structures i and ii). The 2D classification of HTL-SecD$_{D519N}$ shows the open state is populated to a similar extent compared to the unmodified HTL (Figure 6 –figure supplement 1).

The 3D analysis shows the compact states in both cases, similar to those seen before [36] (Figure 3, structure i; Figure 6, structures i and iv). However, the 'open' states are significantly different: blocking the proton pathway in SecD results in a shorter extension of the periplasmic domains of the HTL, compared to the native version (Figure 6, structures ii *versus* v). This is consistent with the conformational change observed at atomic resolution in SecDF alone (Figure 6, structures iii *versus* vi) [28]. Even at the current low-resolution description of the HTL-BAM complex (Figure 2), it is clear that these observed PMF-dependent conformational changes of SecD would be communicated to the outer membrane.

DISCUSSION

The *in vivo* and *in vitro* analyses described here demonstrate a direct, functional interaction between the Sec and BAM translocons, mediated by the extended periplasmic domains possessed by BAM [38], SecDF [28] and YidC [45], but not SecYEG [17]. Evidently, direct contact between HTL and BAM is required for efficient OMP biogenesis in rapidly growing cells. The interaction could enable large protein fluxes to stream through the periplasm, while

minimising aggregation and proteolysis (Figure 7). The presence of super-complexes that bridge both membranes appears to be a fundamental feature of the Gram negative bacterial cell envelope – critical for a whole range of activities including the export of proteins through a gamut of different secretion systems (*e.g.* type I, II, III, IV and VI) [16]; now including the Sec machinery. The general importance of these inter-membrane associations is only just coming to the fore [46,47].

It has already been shown that the HTL contains a lipid-containing cavity within the membrane, presumably to facilitate membrane protein insertion [36,39]. Remarkably also, in the super-complex between HTL and BAM there is a much larger extension of this cavity opening into the periplasm (Figure 2). This would seem an obvious place for OMP passage and for the interaction with chaperones (Figure 7), and is of sufficient size to do so. The cavity is situated such that a secretory protein could enter *via* the protein-channel through SecYEG, and then exit accordingly into the periplasm, or into the mouth of the BAM complex.

It remains to be seen how the Sec-BAM complex and the periplasmic chaperones coordinate. Perhaps these chaperones recognise emerging globular proteins at the Sec-machinery and shuttle them into the periplasm, with or without the need for the BAM complex. Otherwise, they could facilitate passage of OMPs through the inter-membrane assembly for outer-membrane folding and insertion by BAM (Figure 7). SurA is known to interact with BamA [9], and an interaction with the HTL also seems likely (Figure 7). Other ancillary factors of the Sec machinery have also been implicated: YfgM and PpiD are thought to mediate interactions between emergent periplasmic proteins and chaperones [48]; indeed PpiD has also been shown to interact with SecYEG and YidC [49]. Interestingly, *yfgL* and *yfgM* are in the same operon [50], the former encoding a subunit of the BAM complex (BamB) [11]. Indeed, a recent proteomic analysis of the *E. coli* 'membrane protein interactome' identifies cross-membrane interactions involving SecYEG, BAM and the chaperones YfgM and PpiD [51]. Understanding the interplay of various periplasmic chaperones during OMP passage through the Sec-BAM assembly to the outer membrane will require further attention.

From our data it is clear that the periplasmic domain of SecD is central to the physical BAM-HTL interaction. Even more intriguing though is the requirement for a functioning proton wire through the SecDF trans-membrane domain. The non-functioning SecDF is fully capable of conferring an interaction with BAM, but is presumably unable to transmit PMF dependent

conformational changes relayed from the inner-membrane. This static interaction of HTL and BAM is insuffient to enable efficient OMP maturation. The consequences of preventing PMF inducing dynamic interplay between HTL and BAM are as severe as the disconnection induced by SecDF depletion. Presumably, the deletion of the periplasmic domain P1 of SecD, which also eliminates the interaction with the outer-membrane, has an equally severe effect.

The requirement for PMF driven inter-membrane dynamic connectivity raises the intriguing prospect of TonB-style energy-coupling from the inner-membrane [52]: *i.e.* the transmission of free energy available from the PMF *via* the Sec-machinery [2,27,53] for OMP folding and insertion at the outer-membrane. We therefore propose that one of the primary roles of SecDF is in inter-membrane trafficking and energy transduction. Indeed, we and others have shown that ATP- and PMF-driven transport of proteins through the inner membrane is dependent only on SecYEG and SecA [2,19], while we show here that proton translocation through SecD is crucial for efficient OMP folding and growth.

Thus, there appears to be two distinct requirements of the PMF in protein secretion: one for the early stage – SecA driven translocation through SecYEG at the inner membrane, and another for late stages of OMP maturation. The latter facilitated by conformational changes in SecDF for transduction of energy from the inner to the outer membrane. Here, we show that an 'open' state of the HTL interacts with the BAM complex, and that the periplasmic regions of SecD can adopt different conformations, reminiscent of those previously characterised as the *I*- and *F*-forms [28]; when a key proton carrying residue of the inner membrane segment of the translocon is neutralised – $SecD_{D519N}$ – the periplasmic domain adopts the *F*-form [28]. Thus, successive protonation (approximated by $SecD_{D519N}$) and deprotonation result in large, cyclical movements – between the *I*- and *F*-forms – during PMF driven proton transport from the periplasm to the cytosol. Presumably then, the occurance of these conformational changes, while connected to the BAM complex, results in long-range energetic coupling between the inner- and outer-membranes. Interestingly, the phospholipid cardiolipin (CL) is important for the stabilisation of the 'open' state of the HTL and its interaction with the BAM machinery. It is probably not a coincidence that this lipid has already been shown to be critical for PMF-driven protein translocation through SecYEG [32]. Certainly, we hope to overcome the inherent flexibility of the CL-stabilised open translocon, primed to receive BAM, in order to determine its high-resolution structure, and further understand this process.

Taking all together, this builds a compelling case for SecD mediated inter-membrane energy transduction – in keeping with other members of the RND transporter family, such as the assembly of AcrAB (inner-membrane) and TolC (outer-membrane) [54,55]. Direct association between inner- and outer-membrane components appears to be the rule rather than the exception for transporters embedded in double membrane systems: parallels with the translocation assembly module (TAM) for auto-transporter secretion [56], and the TIC-TOC import machinery of chloroplasts [57] are striking, given the respective outer-membrane components (TamA and TOC75) are homologous of BamA. Particularly intriguing is the possibility of the mitochondrial homologue of BAM (Sorting and Assembly Machinery; SAM) participating in analogous inter-membrane interactions between inner- and outer-membranes. Indeed, subunits of the MItochondrial contact site and Cristae Organizing System (MICOS) connect the energy-transducing ATP synthase of the inner-membrane and SAM at the outer-membrane [58,59].

MATERIALS AND METHODS

Strains and plasmids

E. coli C43 (DE3) was a gift from Sir John Walker (MRC Mitochondrial Biology Unit, Cambridge, UK) [60]. *E. coli* BL21 (DE3) were purchased as competent cells (New England Biolabs). *E. coli ΔsecG* (KN425 (W3110 M25 *ΔsecG*::kan)) [31], which lacks a genomic copy of *secG*, was obtained from Prof. Frank Duong (University of British Colombia, Vancouver, Canada). *E. coli* strain JP352 (Kan^r), which contains an arabinose-regulated *secDF-yajC* operon [21], was given to us by Prof. Ross Dalbey.

The plasmids for over-expression of *secEYG* and *yidC* were from our laboratory collection [61,62], the former and also that of *secDF* were acquired from Prof. Frank Duong [18]. Vectors designed for over-production of HTL, HTL(ΔYidC) and HTL($SecD_{D519N}$) were created using the ACEMBL expression systemz [36,63]. The vector for *bamABCDE* over-expression pJH114 (Amp^r) was a gift from Prof. Harris Bernstein [64] from which pJH114-*bamACDE* (ΔBamB) was produced by linear PCR with primers designed to flank the BamB gene and amplify DNA around it. FseI restriction sites were included in the primers to ligate the amplified DNA. pBAD-

SecDF(ΔP1) was generated by amplifying SecDF(ΔP1) from pBAD-SecDF and cloning it between the pBAD NcoI and HindIII sites. [66]

For SecDF depletion experiments, SecDF was cloned into pTrc99a (Amp^r, IPTG-inducible), and the *secD*$_{D519N}$ mutation was subsequently made by changing the WT carrying plasmid using a site-directed ligase-independent PCR method.

SDS-PAGE, western blotting and antibodies

All SDS-PAGE was performed with either *Invitrogen* Bolt 4-12% Bis-Tris gels or *Invitrogen* midi 4-12% Bis-Tris gels. For western blotting, proteins were transferred onto nitrocellulose membrane. Mouse monoclonal antibodies against SecY, SecE and SecG were from our laboratory collection (used at 1:10000 dilution). Polyclonal antibodies against SecD and BamA were generated commercially in rabbits (all used at 1:5000 dilution). BamB and BamD antibodies were gifts from Dr Harris Bertstein (1:5000 dilution). A secondary antibody conjugated to DyLight800 was used for SecG and SecY (Thermo Fisher Scientific, 1:10000 dilution), whereas a HRP-conjugated secondary antibody was used for SecD and BamA (1:10000 dilution).

Protein production and purification

HTL, HTL(ΔYidC), HTL(SecD$_{D519N}$), SecYEG, YidC, and SecDF were purified as described previously [19,61,62,65]. BAM and BAM(ΔBamB) was over-produced in *E. coli* C43 according to established protocols [14,64]. [68]

Isolation of inner and outer membranes

1 L of *E. coli* cultures over-producing SecYEG, HTL, SecDF or SecDF(ΔP1) were produced as described previously [19,61,66]. The harvested cell pellets were resuspended in 20 mL TS$_{130}$G, homogenised with a potter, passed twice through a cell disruptor (Constant Systems Ltd.) for lysis and centrifuged to remove debris (SS34 rotor, Sorvall, 12,000 x*g*, 20 minutes, 4°C). The supernatant was taken and layered upon 20 mL TS$_{130}$G + 20% (w/v) sucrose in a Ti45 tube and centrifuged (Ti45 rotor, Beckmann-Coulter, 167,000 x*g*, 120 minutes, 4°C). The pellet was taken, resuspended in 4 mL TS$_{130}$G, homogenised with a potter and layered upon a sucrose gradient prepared in an SW32 centrifuge tube composed of 5 mL layers of TS$_{130}$G + 55% (w/v), 48%, 41%, 34% and 28% sucrose. The sample was then fractionated by centrifugation (SW32 rotor,

Beckmann-Coulter, 130,000 x*g*, 15 hours, 4°C). Upon completion, the light to heavy fractions were analysed by SDS PAGE and western blotting.

Co-immunoprecipitations (co-IPs) with *E. coli* total membrane extracts

Membrane pellets of *E. coli* strains C43 (WT), C43 pJH114-*bamABCDE* (Amp^r), *ΔsecG* (Kan^r), WT *lpp*, mutant lpp_{+21} and JP325 (containing variants of pTrc as specified in text, cultures grown in glucose for depletion of endogenous SecDFyajC), were prepared as described previously [61], with *bamABCDE* over-expression achieved as before [64]. The pellets were resuspended in $TS_{130}G$ to 120 mg/mL, homogenised and solubilised with 0.5% DDM for 1 hour at 4°C. The solubilised material was clarified by ultra-centrifugation (160,000 x*g* for 45 mins) and the membrane extracts were analysed.

For co-IPs pulling on SecG antibody, 250 µL of protein G resin was washed in a spin column with 200 mM NaCl, 20 mM HEPES pH 8.0 (HS buffer), and blocked overnight in HS buffer + 2% (w/v) BSA at 4°C. Meanwhile, 7.5 µL of purified SecG monoclonal antibody was added to 500 µL of the membrane extracts and incubated overnight at 4°C. The following morning, the resin was washed thoroughly in HS buffer containing either 0.02% (w/v) DDM or 0.02% (w/v) DDM with 0.002% (w/v) CL, resuspended back to 250 µL and added to the 500 µL of membrane extract for three hours rotating gently at room temperature. The resin was separated from the extracts by centrifugation in a spin column at 500 x*g* for 1 minute, washed 6 times with 350 µL HS buffer, followed by one final wash with 150 µL HS buffer, which was collected in a fresh tube for analysis (to which 50 uL of 4x LDS sample buffer was added once collected). The bound material was then eluted by addition of 150 uL 1 x LDS sample buffer (to which an additional 50 uL of 1x LDS sample buffer was added once collected). Samples were analysed by SDS PAGE and western blotting.

For co-affinity adsorption by pulling on the hexa-histidine tag of recombinant BamA, 100 µL of nickel-charged chelating resin was added to 500 µL of membrane extracts and incubated for 5 minutes at room temperature. The resin was then separated from the extract and treated in the same way as described above but with $TS_{130}G$ + 0.02% (w/v) DDM + 0.002% (w/v) CL + 30 mM imidazole (washing) or 300 mM imidazole (elution).

Statistical analyses were conducted using GraphPad Prism. An unpaired T-test was used to compare pull down samples (p-value = 0.05, * = < 0.05, ** = < 0.01, *** = < 0.001, specific p-values are stated in figure legends).

In vitro assembly and purification of complexes for EM and XL-MS

All protein complexes visualized by negative stain EM were formed by incubating 5 µM of the respective proteins in binding buffer (20 mM HEPES pH 8.0, 250 mM NaCl, 0.03% (w/v) DDM, 0.003% (w/v) CL at 30ºC for 30 minutes with shaking in a total volume of 150 µL. The protein complexes were purified in a glycerol/glutaraldehyde gradient (20 - 40% (w/v) and 0 - 0.15% (w/v), respectively) by centrifugation at 34,000 RPM in a SW60 Ti rotor (Beckmann-Coulter) for 16 hours at 4ºC. Mobility controls of individual and partial complexes (BAM, and HTL) or individual proteins (SecYEG, YidC, SecDF) without the glutaraldehyde gradient were performed under the same conditions. Gradients were fractionated in 150 µL aliquots and those with glutaraldehyde were inactivated with 50 mM of Tris pH 8.0. Aliquots were analysed by SDS-PAGE and silver staining.

The HTL:BAM complex for cryoEM was formed by incubating 8 µM of the HTL and BAM complexes in binding buffer (50 mM HEPES pH 8.0, 200 mM NaCl, 0.01% (w/v) DDM / 0.001% (w/v) CL at 30ºC for 20 minutes with shaking in a total volume of 250 µL. After 20 min, 0.05% of glutaraldehyde was added to the sample and incubated for 10 minutes at 21ºC. The crosslinker was inactivated with 30 mM Tris pH 8.0 and the sample was loaded onto a Superose 6 Increase 10/300 GL (GE healthcare) column equilibrated in GF buffer (30 mM Tris pH 8.0, 200 mM NaCl, 0.01% (w/v) DDM). Fractions were analysed by SDS-PAGE and silver staining.

The HTL:BAM complex for cross-linked mass spectroscopy (XL-MS) analysis was prepared following the same procedure described for the cryo-EM preparation, but the sample was crosslinked with 1.5 mM DSBU and inactivated with 20 mM of ammonium carbonate pH 8.0 before being loaded onto the gel filtration column.

XL-MS analysis

The DSBU cross-linked HTL:BAM complex was precipitated by methanol and chloroform [67] and the pellet dissolved in 8 M urea. After reduction with 10 mM DTT (one hour at 37ºC) and alkylation with 50 mM iodoacetamide (30 minutes in the dark at RT), the sample was diluted 1:5

with 62.5 mM ammonium hydrogen carbonate and digested with trypsin (1:20 w/w) overnight at 37ºC. Digestion was stopped by the addition of formic acid to a final concentration of 2% (v/v) and the sample split in two equal amounts for fractionation by size exclusion (SEC) and reverse phase C18 at high pH chromatography. A Superdex Peptide 3.2/300 column (GE Healthcare) was used for SEC fractionation by isocratic elution with 30% (v/v) acetonitrile/ 0.1% (v/v) TFA at a flow rate of 50 µL/ min. Fractions were collected every minute from 1.0 mL to 1.7 mL of elution volume. Reverse phase C18 high pH fractionation was carried out on an Acquity UPLC CSH C18 1.7 µm, 1.0 x 100 mm column (Waters) over a gradient of acetonitrile 2-40% (v/v) and ammonium hydrogen bicarbonate 100 mM.

All the fractions were lyophilized and resuspended in 2% (v/v) acetonitrile and 2% (v/v) formic acid for LC–MS/MS analysis. An Ultimate U3000 HPLC (ThermoScientific Dionex, USA) was used to deliver a flow of approximately 300 nL/ min. A C18 Acclaim PepMap100 5 µm, 100 µm × 20 mm nanoViper (ThermoScientific Dionex, USA), trapped the peptides before separation on a C18 Acclaim PepMap100 3 µm, 75 µm × 250 mm nanoViper (ThermoScientific Dionex, USA). Peptides were eluted with a gradient of acetonitrile. The analytical column was directly interfaced *via* a nano-flow electrospray ionisation source, with a hybrid quadrupole orbitrap mass spectrometer (Q-Exactive HF-X, ThermoScientific, USA). MS data were acquired in data-dependent mode. High-resolution full scans (R=120,000, m/z 350-2000) were recorded in the Orbitrap and after CID activation (stepped collision energy 30 ± 3) of the 10 most intense MS peaks, MS/ MS scans (R=45,000) were acquired.

For data analysis, Xcalibur raw files were converted into the MGF format through MSConvert (Proteowizard [68]) and used directly as input files for MeroX [69]. Searches were performed against an ad-hoc protein database containing the sequences of the complexes and a set of randomised decoy sequences generated by the software. The following parameters were set for the searches: maximum number of missed cleavages 3; targeted residues K; minimum peptide length 5 amino acids; variable modifications: carbamidomethyl-Cys (mass shift 57.02146 Da), Met-oxidation (mass shift 15.99491 Da); DSBU modification fragments: 85.05276 Da and 111.03203 (precision: 5 ppm MS [68] and 10 ppm MS [69]); False Discovery Rate cut-off: 5%. Finally, each fragmentation spectra were manually inspected and validated.

EM and image processing

For negative stain, aliquots of sucrose gradient fractions containing the different complexes were applied to glow-discharged (15 s) carbon grids with Cu 300 mesh, washed and stained with 2% (w/ v) uranyl acetate (1 min). Digital images were acquired with two different microscopes; a Tecnai 12 with a Ceta 16M camera (ThermoFisher Scientific) at a digital magnification of 49,000 x and a sampling resolution of 2.04 Å per pixel, and in a Tecnai 12 with a Gatan Camera One View at a digital magnification of 59,400 and a sampling resolution of 2.1 Å per pixel. Image processing was performed using the EM software framework Scipion v1.2 [70]. Several thousand particles were manually and semi-automatic supervised selected as input for automatic particle picking through the XMIPP3 package [71,72]. Particles were then extracted with the Relion v2.1 package [73,74] and classified with a free-pattern maximum-likelihood method (Relion 2D-classification). After manually removing low quality 2D classes, a second round of 2D classification was performed with Relion and XMIPP-CL2D in parallel [75]. Representative 2D averages were used to generate several initial 3D models with the EMAN v2.12 software [76,77]. Extensive rounds of 3D classification were then carried out using Relion 3D-classification due to the heterogeneity of the sample. The most consistent models were used for subsequent 3D classifications. For the final 3D volume refinement, Relion auto-refine or XMIPP3-Projection Matching were used. Resolution was estimated with Fourier shell correlation using 0.143 correlation coefficient criteria [78,79]. See Figure 2 –source data 2 for image processing details.

For CryoEM, appropriate fractions of the glutaraldehyde-crosslinked HTL:BAM complex purified by gel filtration were applied to glow-discharged (20 s) Quantifoil grids (R1.2/R1.3, Cu 300 mesh) with an ultrathin carbon layer (2 nm), blotted and plunged into a liquid ethane chamber in a Leica EM. Two data sets from the same grid were acquired in a FEI Talos Arctica cryo-electron microscope operated at 200 kV and equipped with a K2 detector at calibrated magnification of 79000 x. The first data set with 2056 images recorded, had a 1.75 Å/px sample resolution, dose rate of 2.26 electrons/$Å^2$ and 20 s exposure time fractionated in 40 frames. Defocus values oscillated between -1.5 nm and -3.0 nm. The second data set with 3703 images recorded, had a 0.875 Å/px sample resolution, dose rate of 2.47 electrons/$Å^2$ and 18 s exposure time fractionated in 40 frames. Defocus values oscillated between – 1.0 nm and -2.2 nm. Particles were picked in the same way as for negative stain, and were binned to a 1.75 Å/px sample resolution before merging to the first data set. Image processing was performed using the EM software

framework Scipion v1.2 [70] with a similar strategy to the negative stain-EM samples but also using extensive masking procedures (Figure 2 –figure supplement 4).

All 3D reconstructions were calculated using a home-built workstation (CPU Intel Core i7 7820X, 2x Asus Turbo GTX 1080Ti, 16Gb RAM DDR4) and partial usage of HPC clusters (Bluecrystal 4 and Bluecryo) at the University of Bristol.

Depletion of SecDF-YajC

E. coli strain JP352 was transformed with empty pTrc99a, or the same plasmid, but cloned with either WT *secDF* or s*ecD*$_{D519N}$*F*. Precultures of the strains were prepared in 100 mL 2xYT media supplemented with 0.2% (w/v) arabinose, ampicillin (for pTrc selectivity) and kanamycin (for JP352 selectivity). The following morning, the cells were harvested by centrifugation and resuspended with 50 mL fresh 2xYT (no arabinose). This washing procedure was repeated two more times to remove excess arabinose. Prewarmed (37ºC) 1 L 2xYT cultures containing either 0.2% (w/v) arabinose or 0.5% (w/v) glucose were then inoculated with the preculture such that a final $OD_{600\ nm}$ of 0.05 was achieved. An aliquot was taken every 1.5 hours for 6 hours. Induction of pTrc with IPTG was not necessary as background expression was sufficient to achieve levels of SecD similar to that of JP325 cultured in the presence of arabinose. Periplasmic fractions were produced by preparing spheroplasts [80], centrifuging the samples at 12000 x*g* for 5 minutes, taking the supernatant (a mixture of periplasmic and OM fractions) and removing the OM fraction by ultracentrifugation at 160000 x*g* for 20 minutes. The fractions were then subjected to SDS-PAGE and western blotting.

Measurement of protein transport

Inner membrane vesicles (IMVs) were produced from BL21(DE3) cells overproducing HTL, HTL(SecD$_{D519N}$), SecYEG or with empty pBAD as described previously [32]. Transport experiments with and without PMF were performed in triplicate using established methods [32].

Acknowledgments:

We are particularly grateful for the generosity of Dr Harris Bernstein for the kind gifts of the *bamABCDE* expression construct (pJH114) and antibodies. Thanks to Prof. Daniel Daley for telling us about YfgL and YfgM. We thank Dr Remy Martin for brewing, and for making the HTL *secD*$_{D519N}$*F* mutant. We acknowledge access and support of the Wolfson Bioimaging Facility and the GW4 Facility for High-Resolution Electron Cryo-Microscopy, with particular thanks to Dr Ufuk Borucu. We are grateful to Mr Tom Batstone for the support at the computer cluster BlueCryo.

Funding: This work was funded by the BBSRC (BB/S008349/1 to IC, DWW and SA; BB/N015126/1 to IC and DWW; BB/M003604/1 to IC and SA; SWBioDTP – BB/J014400/1 and BB/J014400/1 to LT), EMBO (Long Term Fellowship – ALTF 710-2015, LTFCOFUND2013 and GA-2013-609409 – to SA) and the Elizabeth Blackwell Institute for Health Research, University of Bristol (Elizabeth Blackwell Bridging fellowship to SA). The GW4 Facility for High-Resolution Electron Cryo-Microscopy was funded by the Wellcome Trust (electron microscope with direct electron detector; 202904/Z/16/Z and 206181/Z/17/Z) and BBSRC (computer cluster; BB/R000484/1).

Author contribution: SA, DWW, LT, WA and IC designed and conducted experiments, assisted by JL; SA, DWW, LT and IC wrote the manuscript; VAMG and BD provided facilities and expertise, and edited the manuscript; EJC and MB, helped with the Lpp experiments – conception, strain provision and text editing; GD and JMS, conducted the XL-MS experiments, processed the data, helped in their description and interpretation; IC, VAMG, BD and MB secured funding; IC led the project.

Declaration: the authors declare no competing interests.

Data and materials availability: All data are available in the main text or the supplementary materials. The HTL-BAM cryo-EM structure has been deposited at the EMDB under the accession number 11240.

FIGURE LEGENDS:

Figure 1: Identification of interactions between HTL and BAM

a. Schematic representation of sucrose gradient centrifugation tube for fractionation of *E. coli* total membranes. Numbers 1-6 indicate the fractions taken for SDS PAGE and immunoblotting shown in **b, c** and **d**.

b, c. Immunoblots of fractions produced as shown in **a** for membranes of **b**: *E. coli* C43 overproducing either SecYEG or HTL or for **c**: *E. coli* C43 with no over-expression, and those over-producing either SecDF or $SecD_{\Delta P1}F$ (lacking the periplasmic domain 1 (P1) of SecD). To help visualise migration shifts, blotting signal was used to quantify relative abundances of proteins of interest in fractions, shown above or below blots as normalised bar charts, where bars from left (pink) to right (yellow) indicate fractions 1 (OM) – 6 (IM) respectively.

d. Co-immuno-precipitations (co-IP) of SecG, SecD and BamA – pulling with the SecG antibody. Pull-downs were conducted with solubilised crude membrane extracts from *E. coli* C43 (WT), a strain lacking SecG (Δ*secG*), and C43 over-producing BAM. Experiments were conducted in the presence (+CL) and absence (-CL) of cardiolipin. L = load (1% total material), W = final wash before elution (to demonstrate proper washing of affinity resin, 17% of total material) and E = elution (17% of total material).

e. Quantification of IPs shown in (**d**). Error bars represent SEM. An unpaired T-test was used to compare samples (p = 0.05, n = 3, * = < 0.05, ** = < 0.01, p values from left to right are 0.4874, 0.8083, 0.0041, 0.0249, 0.0241 and 0.0839). Quantification was performed for cells of *E. coli* C43 (WT) and the same but overproducing BAM (BAM).

f. Affinity pull-down of recombinant BamA-His_6, SecD and SecG by nickel chelation all in the presence of cardiolipin. L, W and E as described in **(d).**

Figure 1 –figure supplement 1: Raw western blots of co-immuno-precipitations and affinity pull downs

a. Coomassie-stained SDS PAGE of sucrose gradient fractions of *E. coli* C43 total membranes from cells over-producing SecYEG or HTL. Left and right gels show untreated and heat denatured (+Δ) samples respectively. Purified controls of SecYEG and YidC are also shown. Yellow asterisks indicate the positions of OmpC/OmpF.

For (**b)** and **(c)**, L = load (1% total material), W = final wash before elution (to demonstrate complete washing of affinity resin, 17% of total material) and E = elution (17% of total material).

b. Co-immunoprecipitations from Figure 1d-e. Experiments were conducted in the presence (+CL) or absence (-CL) of augmented cardiolipin. Experiments were also carried out in the presence (+AB) or absence (-AB) of anti-SecG primary antibody, as a control to assess non-specific binding. Solubilised membranes of 3 cell strains were used: *E. coli* C43, a strain lacking SecG (Δ*secG*), and C43 over-producing BAM.

c. Affinity pull-downs from Figure 1f. Experiments were conducted with nickel-chelated (Ni) or non-chelated (blank) resin as a control to rule out non-specific binding.

Figure 2: 3D characterization of HTL-BAM by negative stain-EM and cryo-EM in detergent solution, and XL-MS analysis

a. Silver-stained SDS-PAGE gels of fractions from glycerol centrifugation gradients, with increasingly large complexes appearing in fractions of higher percentage glycerol, (from left to right). Gels of BAM alone (top) HTL alone (middle) and HTL mixed with BAM (bottom) are shown. The fractions of furthest migration of the individual components, as determined in the top two gels, are marked by vertical lines. HTLBAM components in heavy fractions are marked with a yellow asterisk.

b. Negative stain analysis of the HTL-BAM complex (37.2 Å resolution) in four representative orthogonal views, with the orientation with respect to the inner and outer membranes inferred. BAM (grey), BamB (orange), SecYEG (cyan), YidC (pink) and SecDF (green) are shown.

c. Three orthogonal views of the cryo-EM HTL-BAM complex 3D reconstruction (18 Å resolution). Colours are as in (**a)**, but with BamA in blue.

d. Side views of the cryo HTL-BAM complex showing the large cavity between the IM and OM complexes.

e. Close-up of the outer-membrane region of the HTL-BAM complex. The cryo-EM structure (transparent surface) with BamABCDE atomic structures docked (pdb_5d0q). The position of BamB (orange) was determined directly by negative stain-EM (Figure 2 –figure supplement 3e). BamA (blue), BamC (yellow), BamD (red) and BamE (pink) are docked according to the HTL-BAM cryo-EM density and XLMS data (Figure 2 –figure supplement 5c). Green sphere atoms in BamC and BamD show interacting points with SecD identified by mass apectrometry.

f. Lower threshold map of HTL-BAM overlaid with the standard threshhold (transparent grey), with the main components coloured as in (**a**). The lateral gate (LG) into the membrane, protein-channel through SecY and the central lipid pool are highlighted.

Figure 2 –figure supplement 1: Glycerol centrifugation gradients of HTL and BAM components

a, b, c. Silver-stained SDS-PAGE gels of fractions from the glycerol centrifugation gradients are shown, with increasingly large complexes appearing in fractions of higher percentage glycerol, (from left to right). For each panel, the glycerol centrifugation gradient of BAM alone is shown (top). The middle gel represents a HTL component (labelled on the top left of the gel). The bottom gel represents the experiment where BAM was mixed with the corresponding HTL component. Dashed lines represent the fraction of furthest migration of the individual components, as determined in the top two gels. Components of HTLBAM in heavy fractions are indicated by yellow asterisks.

Figure 2 –figure supplement 2: Negative-stained EM micrographs of the HTL:BAM complex

a, b, c. Electron micrographs of HTL-BAM complexes in different conditions. Bottom, reference-free (RF) class averages of the largest populations found in the micrographs (top). Micrograph scale bar, 1000 Å. RF scale bar, 100 Å. White arrows indicate representative HTL:BAM complexes used for image processing.

Figure 2 –figure supplement 3: 3D characterization and subunit assignment of HTL-BAM by negative stain-EM in detergent solution

a. Silver stained SDS-PAGE analysis of HTL-BAM fractionated by glycerol density gradient centrifugation (left). Experiment is the same as that shown in Figure 2a (bottom panel), but with GraFix treatment. Black asterisk (left panel) marks the fraction chosen for negative stain EM and image processing. For identification of HTL and BAM components by mass spectrometry, the PAGE sample marked with the black asterisk (left panel) was subjected to a longer running time to further purify bands for cutting (right panel).

b. Top left, four orthogonal views of the HTL-BAM complex 3D reconstruction (37.2 Å resolution). Bottom, reference-free (RF) class averages and projections (P) of the final model, shown in the same orientations as the top. Scale bar, 100 Å. See Figure 2 –source data 2 for image processing details. Right, angular distribution and Fourier shell correlation of the HTL-BAM complex.

For **(c-e)**, top panel shows orthogonal views of different 3D reconstructions, labelled accordingly. Middle panel shows reconstructions superimposed with HTL-BAM (transparent grey) from (**b),** and bottom shows a comparison of the reference-free (RF) class averages of HTL-BAM with the corresponding structure. Scale bar, 100 Å. See Figure 2 –source data 2 or image processing details.

c. SecYEG-SecDF-BAM (without YidC) complex 3D reconstruction (36.7 Å resolution, pink). Pink arrow indicates the mass in HTL-BAM (grey transparent) corresponding to YidC.

d. SecDF-BAM (without SecYEG and YidC) complex 3D reconstruction (39.4 Å resolution, green). Masses for SecDF trans-membrane domain (green arrow) and periplasmic region (red arrow), SecYEG (blue arrow) and YidC (pink arrow) are indicated.

e. HTL-BAM(ΔBamB) complex 3D reconstruction (33.6 Å resolution, orange). Mass corresponding to BamB (orange arrow) and YidC (pink arrow) are indicated.

Figure 2 –figure supplement 4: Image processing and classification strategy for the cryo-EM data of the HTL-BAM complex

Relion 2D classification was used to clean the two preliminary datasets and classify the images. Of Set I, 82% of the particles were used for extensive 3D classifications and auto-refinements. Of Set II, 65% of the particles followed same procedure. High-quality particles from both data sets were grouped and classified again masking the most variable regions. The final stable volume was formed by 8,448 particles (1.3% of the particles), indicative of the number of different sub-

populations found in the sample. The final post-processing structure (Relion 2.0) has an overall resolution of 18.23 Å.

Figure 2 –figure supplement 5: Sample preparation and XL-MS analysis of HTL-BAM

a. Top, Gel filtration chromatography elution profile (Superose 6) of the HTL-BAM complex for cryo-EM and XL-MS analysis. Bottom, silver stained SDS-PAGE gel of the fractions eluted from the gel filtration at the top. Black asterisk marks the fraction used for XL-MS, and a similar sample was used for cryo-EM.

b. Representation of the interaction network between HTL and BAM determined from XL-MS analysis. Internal green lines represent interprotein connections between HTL-HTL, HTL-BAM and BAM-BAM components. Purple lines represent intraprotein connections between the individual subunits of HTL and BAM.

c. Representation of inter-protein interactions between HTL and BAM as determined by XL-MS. The specific crosslink residues are mapped onto the structures of the BAM complex (emd_4061 and pdb_5ayw) and the model of the HTL complex (emd_3506 and pdb_5mg3) [36]. Left, green dots and dashed lines represent positions and interactions, respectively, between SecD residues and BAM components. Yellow, positions and interactions between SecF and BAM components. Right, pink dots and dashed lines represent positions and interactions, respectively, between YidC residues and BAM components. The HTL and BAM structures have been placed artificially separate from one another to best illustrate the cross-linking contacts (rather than to reflect their actual position in the super-complex).

Figure 2 –source data 1: Mass spectrometry analysis of the GraFix fractions for image processing

Analysis of the protein composition of the HTL-BAM preparations in detergent solution by MS. Only proteins of interest are shown in this table. The SDS-PAGE bands corresponding to the GraFix fractions used for negative stain-EM processing (*e.g.* Figure 2 –figure supplement 3a, middle and right, asterisk) were cut from the gel and prepared for protein digestion, extraction and MS.

Figure 2 –source data 2: Parameters of EM analysis of HTL and HTL-BAM structures

Figure 3: EM structures of HTL in ‘compact’ and ‘open’ states

Structure and docking of a previously published cryo-EM structure of HTL in the compact state **(i)** HTL [36], the HTL-BAM complex **(ii)**, HTL in the ‘compact’ state **(iii)** and HTL in the ‘open’ state **(iv)**; structures **(ii - iv)** are from this study.

Figure 3 –figure supplement 1: EM field of wild-type HTL in different conditions

Bottom, reference-free (RF) class averages of the ‘compact’ (comp) and ‘open’ populations found in the micrographs. Percentages of the populations are indicated on the right of the RF images. Micrograph scale bar, 1000 Å. RF scale bar, 100 Å. The conditions used for sample preparation are stated above micrographs.

Figure 4: Effect of increasing periplasmic distance on the HTL-BAM interaction

a. Negative-stain EM model of HTL-BAM (from Figure 2a), annotated with membranes at the experimentally determined distances between the inner and outer membranes of *E. coli* strains containing wild type *lpp* and mutant *lpp*$^{+21}$ [41].

b. Co-immunoprecipitation of SecG, SecD and BamA when pulling from an anti-SecG monoclonal antibody. Co-IPs were conducted in the presence of cardiolipin as in Figure 1d, but with solubilised membranes of strains described in **(a).**

c. Quantification of IPs from **(b)**. Error bars represent SEM. An unpaired T-test was used to compare samples (p = 0.05, n = 3, * = < 0.05, *** = < 0.001, p values from left to right are 0.0170, 0.0990 and 0.0006).

Figure 4 –figure supplement 1: Raw western blots of IPs investigating how periplasmic width effects the HTL-BAM interaction

Legend is the same as described for Figure 1 –figure supplement 1a, but the cell strains used here were either *E. coli* containing WT *lpp* or the mutant *lpp*$^{+21}$. All IPs were conducted in the presence of cardiolipin.

Figure 5: Effects of SecD depletion upon cell growth, OmpA secretion and maturation

a. Western blot illustrating depletion of SecD in *E. coli* JP325 whole cells when grown in the presence of arabinose or glucose. t=0 represents the time at which an overnight culture (grown in arabinose) was used to inoculate a secondary culture containing either arabinose or glucose.

b. Growth of *E. coli* JP325 transformed with empty vector (pTrc99a, 1 + 2), pTrc99a-*secDF* (3 + 4) and pTrc99A-*secD*$_{D519N}$*F* (5 + 6). Primary cultures were prepared in permissive conditions (arabinose). Cells were then washed and plated onto LB-arabinose (left panel) or LB-glucose (non-permissive, right panel).

c. Classical SecA-driven import assay with *E. coli* inner membrane vesicles (IMVs) and OmpA. IMVs contained over-produced protein as stated on the x-axis. Error bars represent SEM (n=3).

d. Periplasmic fractions of *E. coli* JP325 immunoblotted for OmpA. Folded OmpA (bottom band fOmpA) and unfolded OmpA (top band,yellow asterisk; ufOmpA) are shown. Also shown are control lanes containing *E. coli* whole cells with over-produced, mainly 'folded' OmpA (fOmpA, bottom band) and the same sample, but boiled, to produce 'unfolded' OmpA (ufOmpA, top band).

For **(e-g)**, samples were prepared from various cell cultures; see key (inset (**e)**) for strains used. Error bars represent SEM (n=3 for experimental samples grown in glucose).

e. Quantification of SecD from western blots such as those shown in **(a)** (Figure 5 –figure supplement 1a). Values are normalised to JP325-pTrc99a at t = 0.

f. Culture growth curves.

g. Analysis of western blots such as those from **(d)** and Figure 5 –figure supplement 1d showing the quantity of ufOmpA as a fraction of the total OmpA in the periplasmic fraction.

h. Representative western blots of co-immuno-precipitations conducted as in Figure 1d in the presence of CL, but with solubilised membranes prepared from *E. coli JP325* grown in the presence of glucose and cloned with variants of pTrc99a, as stated in the figure.

i. Quantification of BamA pull down from co-IPs shown in **(h)**. Error bars represent SEM. An unpaired T-test was used to compare samples (p = 0.05, n = 3, * = < 0.05, p values from left to right are 0.0449 and 0.6412).

Figure 5 –figure supplement 1: Raw western blots accompanying SecD depletion experiments from Figure 5

a. Western blots of whole cells visualised for SecD. Cell strains used were *E. coli* JP325 containing either empty pTrc99a, pTrc99a-SecDF or pTrc99a-SecD$_{D519N}$F. A preculture of JP325 was grown in arabinose. Cells were washed and then used to inoculate secondary cultures containing either arabinose (permissive) or glucose (non-permissive), as indicated in the figure. R1/2/3 represent samples taken from replicate cultures. These blots were quantified to give Figure 5f.

b. Immunoblotting of SecY in inverted membrane vesicles used in Figure 5c. Samples were prepared at 4 dilutions: neat (1), ½ (2), ¼ (3) and 1/8 (4). SecY is indicated at the expected apparent Mw of 30 kDa. A higher band is also present at approximately 50 kDa, likely due to SecY dimers.

c. OmpA western blots of periplasmic fractions of *E. coli* JP325 as prepared in **(a),** but with cells containing no plasmid. Three controls are shown: first, *E. coli* BL21 whole cells containing overproduced OmpA with no treatment (-, lane2) and with boiling (+, lane 3) to illustrate the presence of fOmpA and ufOmpA; second, purified proOmpA (lane 4); and third, a whole cell fraction of a preculture of the JP325 parent strain, MC4100, grown in the presence of arabinose. Red asterisks indicate an unknown OmpA intermediate (discussed in main text).

d. OmpA western blots of periplasmic fractions of cells from **(a).** Unfolded (ufOmpA) and folded OmpA (fOmpA) are indicated. These blots were quantified to give Figure 5i.

e. BamA western blot of whole JP325 taken from cultures grown during depletion of SecDF-yajC, as described in (**a**).

f. Raw western blots of co-IPs conducted in Figure 5e-f. Legend is the same as for Figure 1 – figure supplement 1a, except the membranes used here were from strains described in **(a**), all grown in the presence of glucose for depletion of endogeneous SecDF-yajC. All IPs were conducted in the presence of cardiolipin.

g. Quantification of SecG and SecD from co-IPs shown in **(f)**. An unpaired t-test was used to compare samples (p = 0.05, n = 3, * = < 0.05, *** = < 0.001, p values from left to right are 0.0.1391, 0.0137, 0.0001 and 0.3618).

Figure 6: Structural comparison of HTL and HTL519.

Comparison of negative stain-EM structures of 'compact' (structures i and iv) and 'open' (structures ii and v) conformations of HTL *versus* the counterpart containing $SecD_{D519N}F$ (HTL519), both in the presence of CL. Atomic structures of SecDF overlaid with filtered maps at 5 Å are shown alongside for the *I*-form (structure iii, 3XAM) and *F*-form (structure vi, 3AQP), with the amino acid substitution equivalent to the *E.coli* $SecD_{D519N}$, 3AQP). The grey arbitrary mass indicates the approximate position and mass of SecYEG.

Figure 6 –figure supplement 1: Negative-stain EM of HTL containing $SecD_{D519N}$ (HTL519)

Electron micrographs of wild type (wt) HTL and HTL containing $SecD_{D519N}F$ (HTL519) in the same conditions (with cardiolipin, and without GraFix). Bottom, reference-free (RF) class averages of the 'compact' (comp) and 'open' populations found in the micrographs (top). Percentages of the populations are indicated on the right of RF images. Micrograph scale bar, 1000 Å. RF scale bar, 100 Å.

Figure 7: Schematic representation of the HTL:BAM machinery

Schematic model of OMP transfer through the bacterial envelope, facilitated by HTL-BAM and periplasmic chaperones, such as SurA, Skp, PpiD and YfgM. From left to right: OMP precursors with an N-terminal signal sequence are driven across the membrane by the ATPase SecA through the Sec translocon – the process is stimulated by PMF (independent of SecDF). Late in this process the pre-protein emerges into the periplasm and the signal sequence is removed, releasing the mature protein. Presumably, globular proteins are then guided into the periplasm, where folding will occur assisted by periplasmic chaperones. Otherwise, OMP-chaperone-HTL complexes are recognised by the BAM complex, with interactions forming between BAM and both HTL (this study) and SurA [9]. The persistence and variety of chaperones involvement at this stage is unclear (?). This conjunction enables the smooth and efficient passage of OMPs to the outer-membrane, which is enabled by energy coupling of the inner membrane proton motive force with conformational changes in the periplasmic domain of SecDF (right).

REFERENCES:

[1] A. Konovalova, D.E. Kahne, T.J. Silhavy, Outer Membrane Biogenesis., Annual Review of Microbiology. 71 (2017) 539–556. https://doi.org/10.1146/annurev-micro-090816-093754.

[2] L. Brundage, J.P. Hendrick, E. Schiebel, A.J. Driessen, W. Wickner, The purified E. coli integral membrane protein SecY/E is sufficient for reconstitution of SecA-dependent precursor protein translocation., Cell. 62 (1990) 649–657.

[3] I. Collinson, The Dynamic ATP-Driven Mechanism of Bacterial Protein Translocation and the Critical Role of Phospholipids., Frontiers in Microbiology. 10 (2019) 1217. https://doi.org/10.3389/fmicb.2019.01217.

[4] R. Lill, K. Cunningham, L.A. Brundage, K. Ito, D. Oliver, W. Wickner, SecA protein hydrolyzes ATP and is an essential component of the protein translocation ATPase of Escherichia coli., The EMBO Journal. 8 (1989) 961–966.

[5] T. Cranford-Smith, D. Huber, The way is the goal: how SecA transports proteins across the cytoplasmic membrane in bacteria., FEMS Microbiology Letters. 365 (2018). https://doi.org/10.1093/femsle/fny093.

[6] L.G. Josefsson, L.L. Randall, Different exported proteins in E. coli show differences in the temporal mode of processing in vivo., Cell. 25 (1981) 151–157.

[7] C.N. Chang, G. Blobel, P. Model, Detection of prokaryotic signal peptidase in an Escherichia coli membrane fraction: endoproteolytic cleavage of nascent f1 pre-coat protein., Proceedings of the National Academy of Sciences of the United States of America. 75 (1978) 361–365.

[8] L.M. McMorran, A.I. Bartlett, G.H.M. Huysmans, S.E. Radford, D.J. Brockwell, Dissecting the effects of periplasmic chaperones on the in vitro folding of the outer membrane protein PagP., Journal of Molecular Biology. 425 (2013) 3178–3191. https://doi.org/10.1016/j.jmb.2013.06.017.

[9] J.G. Sklar, T. Wu, D. Kahne, T.J. Silhavy, Defining the roles of the periplasmic chaperones SurA, Skp, and DegP in Escherichia coli., Genes & Development. 21 (2007) 2473–2484. https://doi.org/10.1101/gad.1581007.

[10] R. Voulhoux, M.P. Bos, J. Geurtsen, M. Mols, J. Tommassen, Role of a highly conserved bacterial protein in outer membrane protein assembly., Science (New York, N.Y.). 299 (2003) 262–265. https://doi.org/10.1126/science.1078973.

[11] T. Wu, J. Malinverni, N. Ruiz, S. Kim, T.J. Silhavy, D. Kahne, Identification of a multicomponent complex required for outer membrane biogenesis in Escherichia coli., Cell. 121 (2005) 235–245. https://doi.org/10.1016/j.cell.2005.02.015.

[12] J. Bakelar, S.K. Buchanan, N. Noinaj, The structure of the β-barrel assembly machinery complex, Science (New York, N.Y.). 351 (2016) 180–186. https://doi.org/10.1126/science.aad3460.

[13] Y. Gu, H. Li, H. Dong, Y. Zeng, Z. Zhang, N.G. Paterson, P.J. Stansfeld, Z. Wang, Y. Zhang, W. Wang, C. Dong, Structural basis of outer membrane protein insertion by the BAM complex., Nature. 531 (2016) 64–69. https://doi.org/10.1038/nature17199.

[14] M.G. Iadanza, A.J. Higgins, B. Schiffrin, A.N. Calabrese, D.J. Brockwell, A.E. Ashcroft, S.E. Radford, N.A. Ranson, Lateral opening in the intact β-barrel assembly machinery captured by cryo-EM., Nature Communications. 7 (2016) 12865. https://doi.org/10.1038/ncomms12865.

[15] D.P. Ricci, T.J. Silhavy, Outer Membrane Protein Insertion by the β-barrel Assembly Machine., EcoSal Plus. 8 (2019). https://doi.org/10.1128/ecosalplus.esp-0035-2018.

[16] E.R. Green, J. Mecsas, Bacterial Secretion Systems: An Overview., Microbiology Spectrum. 4 (2016). https://doi.org/10.1128/microbiolspec.vmbf-0012-2015.

[17] B.V. den Berg, W.M. Clemons, I. Collinson, Y. Modis, E. Hartmann, S.C. Harrison, T.A. Rapoport, X-ray structure of a protein-conducting channel., Nature. 427 (2004) 36–44. https://doi.org/10.1038/nature02218.

[18] F. Duong, W. Wickner, Distinct catalytic roles of the SecYE, SecG and SecDFyajC subunits of preprotein translocase holoenzyme., The EMBO Journal. 16 (1997) 2756–2768. https://doi.org/10.1093/emboj/16.10.2756.

[19] R.J. Schulze, J. Komar, M. Botte, W.J. Allen, S. Whitehouse, V.A.M. Gold, J.A.L.A. Nijeholt, K. Huard, I. Berger, C. Schaffitzel, I. Collinson, Membrane protein insertion and proton-motive-force-dependent secretion through the bacterial holo-translocon SecYEG-SecDF-YajC-YidC., Proceedings of the National Academy of Sciences of the United States of America. 111 (2014) 4844–4849. https://doi.org/10.1073/pnas.1315901111.

[20] T.T. Tseng, K.S. Gratwick, J. Kollman, D. Park, D.H. Nies, A. Goffeau, M.H. Saier, The RND permease superfamily: an ancient, ubiquitous and diverse family that includes human disease and development proteins., Journal of Molecular Microbiology and Biotechnology. 1 (1999) 107–125.

[21] A. Economou, J.A. Pogliano, J. Beckwith, D.B. Oliver, W. Wickner, SecA membrane cycling at SecYEG is driven by distinct ATP binding and hydrolysis events and is regulated by SecD and SecF., Cell. 83 (1995) 1171–1181.

[22] J.A. Pogliano, J. Beckwith, SecD and SecF facilitate protein export in Escherichia coli., The EMBO Journal. 13 (1994) 554–561.

[23] J.C. Samuelson, M. Chen, F. Jiang, I. Möller, M. Wiedmann, A. Kuhn, G.J. Phillips, R.E. Dalbey, YidC mediates membrane protein insertion in bacteria., Nature. 406 (2000) 637–641. https://doi.org/10.1038/35020586.

[24] P.A. Scotti, M.L. Urbanus, J. Brunner, J.W. de Gier, G. von Heijne, C. van der Does, A.J. Driessen, B. Oudega, J. Luirink, YidC, the Escherichia coli homologue of mitochondrial Oxa1p, is a component of the Sec translocase., The EMBO Journal. 19 (2000) 542–549. https://doi.org/10.1093/emboj/19.4.542.

[25] C. Gardel, S. Benson, J. Hunt, S. Michaelis, J. Beckwith, secD, a new gene involved in protein export in Escherichia coli., Journal of Bacteriology. 169 (1987) 1286–1290.

[26] T. Eicher, M.A. Seeger, C. Anselmi, W. Zhou, L. Brandstätter, F. Verrey, K. Diederichs, J.D. Faraldo-Gómez, K.M. Pos, Coupling of remote alternating-access transport mechanisms for protons and substrates in the multidrug efflux pump AcrB., ELife. 3 (2014). https://doi.org/10.7554/elife.03145.

[27] R.A. Arkowitz, W. Wickner, SecD and SecF are required for the proton electrochemical gradient stimulation of preprotein translocation., The EMBO Journal. 13 (1994) 954–963.

[28] A. Furukawa, K. Yoshikaie, T. Mori, H. Mori, Y.V. Morimoto, Y. Sugano, S. Iwaki, T. Minamino, Y. Sugita, Y. Tanaka, T. Tsukazaki, Tunnel Formation Inferred from the I-Form Structures of the Proton-Driven Protein Secretion Motor SecDF., Cell Reports. 19 (2017) 895–901. https://doi.org/10.1016/j.celrep.2017.04.030.

[29] K. Mio, T. Tsukazaki, H. Mori, M. Kawata, T. Moriya, Y. Sasaki, R. Ishitani, K. Ito, O. Nureki, C. Sato, Conformational variation of the translocon enhancing chaperone SecDF., Journal of Structural and Functional Genomics. 15 (2014) 107–115. https://doi.org/10.1007/s10969-013-9168-4.

[30] T. Tsukazaki, H. Mori, Y. Echizen, R. Ishitani, S. Fukai, T. Tanaka, A. Perederina, D.G. Vassylyev, T. Kohno, A.D. Maturana, K. Ito, O. Nureki, Structure and function of a membrane component SecDF that enhances protein export., Nature. 474 (2011) 235–238. https://doi.org/10.1038/nature09980.

[31] K. Nishiyama, M. Hanada, H. Tokuda, Disruption of the gene encoding p12 (SecG) reveals the direct involvement and important function of SecG in the protein translocation of Escherichia coli at low temperature., The EMBO Journal. 13 (1994) 3272–3277.

[32] R.A. Corey, E. Pyle, W.J. Allen, D.W. Watkins, M. Casiraghi, B. Miroux, I. Arechaga, A. Politis, I. Collinson, Specific cardiolipin-SecY interactions are required for proton-motive force stimulation of protein secretion., Proceedings of the National Academy of Sciences of the United States of America. 115 (2018) 7967–7972. https://doi.org/10.1073/pnas.1721536115.

[33] V.A.M. Gold, A. Robson, H. Bao, T. Romantsov, F. Duong, I. Collinson, The action of cardiolipin on the bacterial translocon., Proceedings of the National Academy of Sciences of the United States of America. 107 (2010) 10044–10049. https://doi.org/10.1073/pnas.0914680107.

[34] D.S. Chorev, L.A. Baker, D. Wu, V. Beilsten-Edmands, S.L. Rouse, T. Zeev-Ben-Mordehai, C. Jiko, F. Samsudin, C. Gerle, S. Khalid, A.G. Stewart, S.J. Matthews, K. Grünewald, C.V. Robinson, Protein assemblies ejected directly from native membranes yield complexes for mass spectrometry., Science (New York, N.Y.). 362 (2018) 829–834. https://doi.org/10.1126/science.aau0976.

[35] B. Kastner, N. Fischer, M.M. Golas, B. Sander, P. Dube, D. Boehringer, K. Hartmuth, J. Deckert, F. Hauer, E. Wolf, H. Uchtenhagen, H. Urlaub, F. Herzog, J.M. Peters, D. Poerschke, R. Lührmann, H. Stark, GraFix: sample preparation for single-particle electron cryomicroscopy., Nature Methods. 5 (2008) 53–55. https://doi.org/10.1038/nmeth1139.

[36] M. Botte, N.R. Zaccai, J.L.À. Nijeholt, R. Martin, K. Knoops, G. Papai, J. Zou, A. Deniaud, M. Karuppasamy, Q. Jiang, A.S. Roy, K. Schulten, P. Schultz, J. Rappsilber, G. Zaccai, I. Berger, I. Collinson, C. Schaffitzel, A central cavity within the holo-translocon suggests a mechanism for membrane protein insertion., Scientific Reports. 6 (2016) 38399. https://doi.org/10.1038/srep38399.

[37] B. Zuber, M. Chami, C. Houssin, J. Dubochet, G. Griffiths, M. Daffé, Direct visualization of the outer membrane of mycobacteria and corynebacteria in their native state., Journal of Bacteriology. 190 (2008) 5672–5680. https://doi.org/10.1128/jb.01919-07.

[38] X. Ma, Q. Wang, Y. Li, P. Tan, H. Wu, P. Wang, X. Dong, L. Hong, G. Meng, How BamA recruits OMP substrates via poly-POTRAs domain., FASEB Journal : Official Publication of the Federation of American Societies for Experimental Biology. (2019) fj201900681RR. https://doi.org/10.1096/fj.201900681rr.

[39] R. Martin, A.H. Larsen, R.A. Corey, S.R. Midtgaard, H. Frielinghaus, C. Schaffitzel, L. Arleth, I. Collinson, Structure and Dynamics of the Central Lipid Pool and Proteins of the Bacterial Holo-Translocon., Biophysical Journal. (2019). https://doi.org/10.1016/j.bpj.2019.04.002.

[40] J.P. Hendrick, W. Wickner, SecA protein needs both acidic phospholipids and SecY/E protein for functional high-affinity binding to the Escherichia coli plasma membrane., The Journal of Biological Chemistry. 266 (1991) 24596–24600.

[41] A.T. Asmar, J.L. Ferreira, E.J. Cohen, S.-H. Cho, M. Beeby, K.T. Hughes, J.-F. Collet, Communication across the bacterial cell envelope depends on the size of the periplasm., PLoS Biology. 15 (2017) e2004303. https://doi.org/10.1371/journal.pbio.2004303.

[42] E.J. Cohen, J.L. Ferreira, M.S. Ladinsky, M. Beeby, K.T. Hughes, Nanoscale-length control of the flagellar driveshaft requires hitting the tethered outer membrane., Science (New York, N.Y.). 356 (2017) 197–200. https://doi.org/10.1126/science.aam6512.

[43] N. Nouwen, A.J.M. Driessen, SecDFyajC forms a heterotetrameric complex with YidC., Molecular Microbiology. 44 (2002) 1397–1405.

[44] P.V. Bulieris, S. Behrens, O. Holst, J.H. Kleinschmidt, Folding and insertion of the outer membrane protein OmpA is assisted by the chaperone Skp and by lipopolysaccharide., The Journal of Biological Chemistry. 278 (2003) 9092–9099. https://doi.org/10.1074/jbc.m211177200.

[45] K. Kumazaki, K. Kumazaki, T. Kishimoto, T. Kishimoto, A. Furukawa, A. Furukawa, H. Mori, H. Mori, Y. Tanaka, Y. Tanaka, N. Dohmae, N. Dohmae, R. Ishitani, R. Ishitani, T. Tsukazaki, T. Tsukazaki, O. Nureki, O. Nureki, Crystal structure of Escherichia coli YidC, a membrane protein chaperone and insertase., Scientific Reports. 4 (2014) 7299. https://doi.org/10.1038/srep07299.

[46] P. Rassam, N.A. Copeland, O. Birkholz, C. Tóth, M. Chavent, A.L. Duncan, S.J. Cross, N.G. Housden, R. Kaminska, U. Seger, D.M. Quinn, T.J. Garrod, M.S.P. Sansom, J. Piehler, C.G. Baumann, C. Kleanthous, Supramolecular assemblies underpin turnover of outer membrane proteins in bacteria., Nature. 523 (2015) 333–336. https://doi.org/10.1038/nature14461.

[47] P. Rassam, K.R. Long, R. Kaminska, D.J. Williams, G. Papadakos, C.G. Baumann, C. Kleanthous, Intermembrane crosstalk drives inner-membrane protein organization in Escherichia coli., Nature Communications. 9 (2018) 1082. https://doi.org/10.1038/s41467-018-03521-4.

[48] H. Götzke, I. Palombo, C. Muheim, E. Perrody, P. Genevaux, R. Kudva, M. Muller, D.O. Daley, YfgM is an ancillary subunit of the SecYEG translocon in Escherichia coli., The Journal of Biological Chemistry. 289 (2014) 19089–19097. https://doi.org/10.1074/jbc.m113.541672.

[49] B. Jauß, N.A. Petriman, F. Drepper, L. Franz, I. Sachelaru, T. Welte, R. Steinberg, B. Warscheid, H.-G. Koch, Non-competitive binding of PpiD and YidC to the SecYEG translocon expands the global view on the SecYEG interactome in E. coli., The Journal of Biological Chemistry. (2019). https://doi.org/10.1074/jbc.ra119.010686.

[50] F.R. Blattner, G. Plunkett, C.A. Bloch, N.T. Perna, V. Burland, M. Riley, J. Collado-Vides, J.D. Glasner, C.K. Rode, G.F. Mayhew, J. Gregor, N.W. Davis, H.A. Kirkpatrick, M.A. Goeden, D.J. Rose, B. Mau, Y. Shao, The complete genome sequence of Escherichia coli K-12., Science (New York, N.Y.). 277 (1997) 1453–1462.

[51] M.L. Carlson, R.G. Stacey, J.W. Young, I.S. Wason, Z. Zhao, D.G. Rattray, N. Scott, C.H. Kerr, M. Babu, L.J. Foster, F.D.V. Hoa, Profiling the Escherichia coli membrane protein interactome captured in Peptidisc libraries., ELife. 8 (2019). https://doi.org/10.7554/elife.46615.

[52] H. Celia, N. Noinaj, S.D. Zakharov, E. Bordignon, I. Botos, M. Santamaria, T.J. Barnard, W.A. Cramer, R. Lloubes, S.K. Buchanan, Structural insight into the role of the Ton complex in energy transduction., Nature. 538 (2016) 60–65. https://doi.org/10.1038/nature19757.

[53] E. Schiebel, A.J. Driessen, F.U. Hartl, W. Wickner, Delta mu H+ and ATP function at different steps of the catalytic cycle of preprotein translocase., Cell. 64 (1991) 927–939.

[54] D. Du, Z. Wang, N.R. James, J.E. Voss, E. Klimont, T. Ohene-Agyei, H. Venter, W. Chiu, B.F. Luisi, Structure of the AcrAB-TolC multidrug efflux pump., Nature. 509 (2014) 512–515. https://doi.org/10.1038/nature13205.

[55] Z. Wang, G. Fan, C.F. Hryc, J.N. Blaza, I.I. Serysheva, M.F. Schmid, W. Chiu, B.F. Luisi, D. Du, An allosteric transport mechanism for the AcrAB-TolC multidrug efflux pump., ELife. 6 (2017). https://doi.org/10.7554/elife.24905.

[56] J. Selkrig, K. Mosbahi, C.T. Webb, M.J. Belousoff, A.J. Perry, T.J. Wells, F. Morris, D.L. Leyton, M. Totsika, M.-D. Phan, N. Celik, M. Kelly, C. Oates, E.L. Hartland, R.M. Robins-Browne, S.H. Ramarathinam, A.W. Purcell, M.A. Schembri, R.A. Strugnell, I.R. Henderson, D. Walker, T. Lithgow, Discovery of an archetypal protein transport system in bacterial outer membranes., Nature Structural & Molecular Biology. 19 (2012) 506-10-S1. https://doi.org/10.1038/nsmb.2261.

[57] Y.-L. Chen, L.-J. Chen, C.-C. Chu, P.-K. Huang, J.-R. Wen, H.-M. Li, TIC236 links the outer and inner membrane translocons of the chloroplast., Nature. (2018). https://doi.org/10.1038/s41586-018-0713-y.

[58] C. Ott, E. Dorsch, M. Fraunholz, S. Straub, V. Kozjak-Pavlovic, Detailed analysis of the human mitochondrial contact site complex indicate a hierarchy of subunits., PloS One. 10 (2015) e0120213. https://doi.org/10.1371/journal.pone.0120213.

[59] H. Rampelt, M. Bohnert, R.M. Zerbes, S.E. Horvath, B. Warscheid, N. Pfanner, M. van der Laan, Mic10, a Core Subunit of the Mitochondrial Contact Site and Cristae Organizing System, Interacts with the Dimeric F1Fo-ATP Synthase., Journal of Molecular Biology. 429 (2017) 1162–1170. https://doi.org/10.1016/j.jmb.2017.03.006.

[60] B. Miroux, J.E. Walker, Over-production of proteins in Escherichia coli: mutant hosts that allow synthesis of some membrane proteins and globular proteins at high levels., Journal of Molecular Biology. 260 (1996) 289–298. https://doi.org/10.1006/jmbi.1996.0399.

[61] I. Collinson, C. Breyton, F. Duong, C. Tziatzios, D. Schubert, E. Or, T. Rapoport, W. Kühlbrandt, Projection structure and oligomeric properties of a bacterial core protein translocase., The EMBO Journal. 20 (2001) 2462–2471. https://doi.org/10.1093/emboj/20.10.2462.

[62] M. Lotz, W. Haase, W. Kühlbrandt, I. Collinson, Projection structure of yidC: a conserved mediator of membrane protein assembly., Journal of Molecular Biology. 375 (2008) 901–907. https://doi.org/10.1016/j.jmb.2007.10.089.

[63] C. Bieniossek, Y. Nie, D. Frey, N. Olieric, C. Schaffitzel, I. Collinson, C. Romier, P. Berger, T.J. Richmond, M.O. Steinmetz, I. Berger, Automated unrestricted multigene

recombineering for multiprotein complex production., Nature Methods. 6 (2009) 447–450. https://doi.org/10.1038/nmeth.1326.

[64] G. Roman-Hernandez, J.H. Peterson, H.D. Bernstein, Reconstitution of bacterial autotransporter assembly using purified components., ELife. 3 (2014) e04234. https://doi.org/10.7554/elife.04234.

[65] B.M. Burmann, C. Wang, S. Hiller, Conformation and dynamics of the periplasmic membrane-protein-chaperone complexes OmpX-Skp and tOmpA-Skp., Nature Structural & Molecular Biology. 20 (2013) 1265–1272. https://doi.org/10.1038/nsmb.2677.

[66] J. Komar, S. Alvira, R.J. Schulze, R. Martin, J.A.L.A. Nijeholt, S.C. Lee, T.R. Dafforn, G. Deckers-Hebestreit, I. Berger, C. Schaffitzel, I. Collinson, Membrane protein insertion and assembly by the bacterial holo-translocon SecYEG-SecDF-YajC-YidC., The Biochemical Journal. 473 (2016) 3341–3354. https://doi.org/10.1042/bcj20160545.

[67] D. Wessel, U.I. Flügge, A method for the quantitative recovery of protein in dilute solution in the presence of detergents and lipids., Analytical Biochemistry. 138 (1984) 141–143. https://doi.org/10.1016/0003-2697(84)90782-6.

[68] D. Kessner, M. Chambers, R. Burke, D. Agus, P. Mallick, ProteoWizard: open source software for rapid proteomics tools development., Bioinformatics (Oxford, England). 24 (2008) 2534–2536. https://doi.org/10.1093/bioinformatics/btn323.

[69] M. Götze, J. Pettelkau, R. Fritzsche, C.H. Ihling, M. Schäfer, A. Sinz, Automated assignment of MS/MS cleavable cross-links in protein 3D-structure analysis., Journal of the American Society for Mass Spectrometry. 26 (2015) 83–97. https://doi.org/10.1007/s13361-014-1001-1.

[70] J.M. de la Rosa-Trevín, A. Quintana, L.D. Cano, A. Zaldívar, I. Foche, J. Gutiérrez, J. Gómez-Blanco, J. Burguet-Castell, J. Cuenca-Alba, V. Abrishami, J. Vargas, J. Otón, G. Sharov, J.L. Vilas, J. Navas, P. Conesa, M. Kazemi, R. Marabini, C.O.S. Sorzano, J.M. Carazo, Scipion: A software framework toward integration, reproducibility and validation in 3D electron microscopy., Journal of Structural Biology. 195 (2016) 93–99. https://doi.org/10.1016/j.jsb.2016.04.010.

[71] V. Abrishami, A. Zaldívar-Peraza, J.M. de la Rosa-Trevín, J. Vargas, J. Otón, R. Marabini, Y. Shkolnisky, J.M. Carazo, C.O.S. Sorzano, A pattern matching approach to the automatic selection of particles from low-contrast electron micrographs., Bioinformatics (Oxford, England). 29 (2013) 2460–2468. https://doi.org/10.1093/bioinformatics/btt429.

[72] J.M. de la Rosa-Trevín, J. Otón, R. Marabini, A. Zaldívar, J. Vargas, J.M. Carazo, C.O.S. Sorzano, Xmipp 3.0: an improved software suite for image processing in electron microscopy., Journal of Structural Biology. 184 (2013) 321–328. https://doi.org/10.1016/j.jsb.2013.09.015.

[73] S.H.W. Scheres, RELION: implementation of a Bayesian approach to cryo-EM structure determination., Journal of Structural Biology. 180 (2012) 519–530. https://doi.org/10.1016/j.jsb.2012.09.006.

[74] D. Kimanius, B.O. Forsberg, S.H. Scheres, E. Lindahl, Accelerated cryo-EM structure determination with parallelisation using GPUs in RELION-2., ELife. 5 (2016). https://doi.org/10.7554/elife.18722.

[75] C.O.S. Sorzano, J.R. Bilbao-Castro, Y. Shkolnisky, M. Alcorlo, R. Melero, G. Caffarena-Fernández, M. Li, G. Xu, R. Marabini, J.M. Carazo, A clustering approach to multireference alignment of single-particle projections in electron microscopy., Journal of Structural Biology. 171 (2010) 197–206. https://doi.org/10.1016/j.jsb.2010.03.011.

[76] S.H.W. Scheres, A Bayesian view on cryo-EM structure determination., Journal of Molecular Biology. 415 (2012) 406–418. https://doi.org/10.1016/j.jmb.2011.11.010.

[77] G. Tang, L. Peng, P.R. Baldwin, D.S. Mann, W. Jiang, I. Rees, S.J. Ludtke, EMAN2: an extensible image processing suite for electron microscopy., Journal of Structural Biology. 157 (2007) 38–46. https://doi.org/10.1016/j.jsb.2006.05.009.

[78] P.B. Rosenthal, R. Henderson, Optimal determination of particle orientation, absolute hand, and contrast loss in single-particle electron cryomicroscopy., Journal of Molecular Biology. 333 (2003) 721–745.

[79] S.H.W. Scheres, S. Chen, Prevention of overfitting in cryo-EM structure determination., Nature Methods. 9 (2012) 853–854. https://doi.org/10.1038/nmeth.2115.

[80] D.C. Birdsell, E.H. Cota-Robles, Production and ultrastructure of lysozyme and ethylenediaminetetraacetate-lysozyme spheroplasts of Escherichia coli., Journal of Bacteriology. 93 (1967) 427–437.

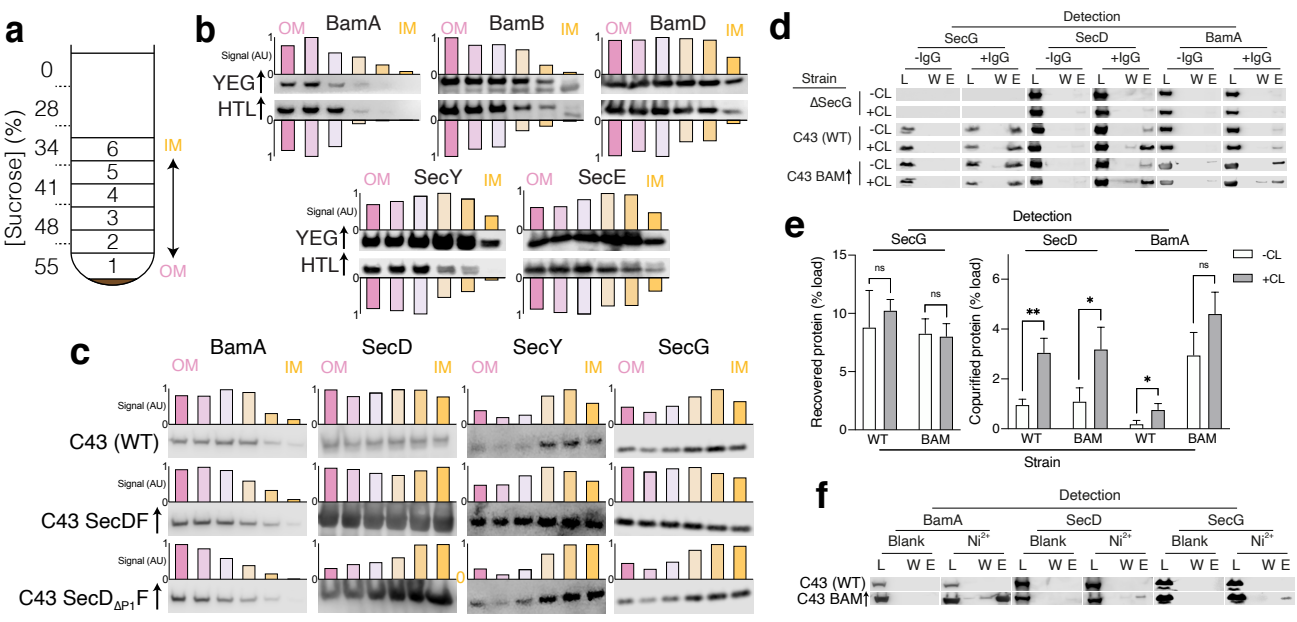
a
[Sucrose] (%)
0
28
34
41
48
55
6
5
4
3
2
1
IM
OM
b
BamA
BamB
BamD
SecY
SecE
OM
IM
Signal (AU)
YEG
HTL
c
BamA
SecD
SecY
SecG
C43 (WT)
C43 SecDF
C43 SecD$_{\Delta P1}$F
d
Detection
SecG
SecD
BamA
-IgG
+IgG
Strain
L W E
ΔSecG
C43 (WT)
C43 BAM↑
-CL
+CL
e
Recovered protein (% load)
Copurified protein (% load)
ns
**
*
WT
BAM
Strain
f
Blank
Ni2+
C43 (WT)
C43 BAM↑

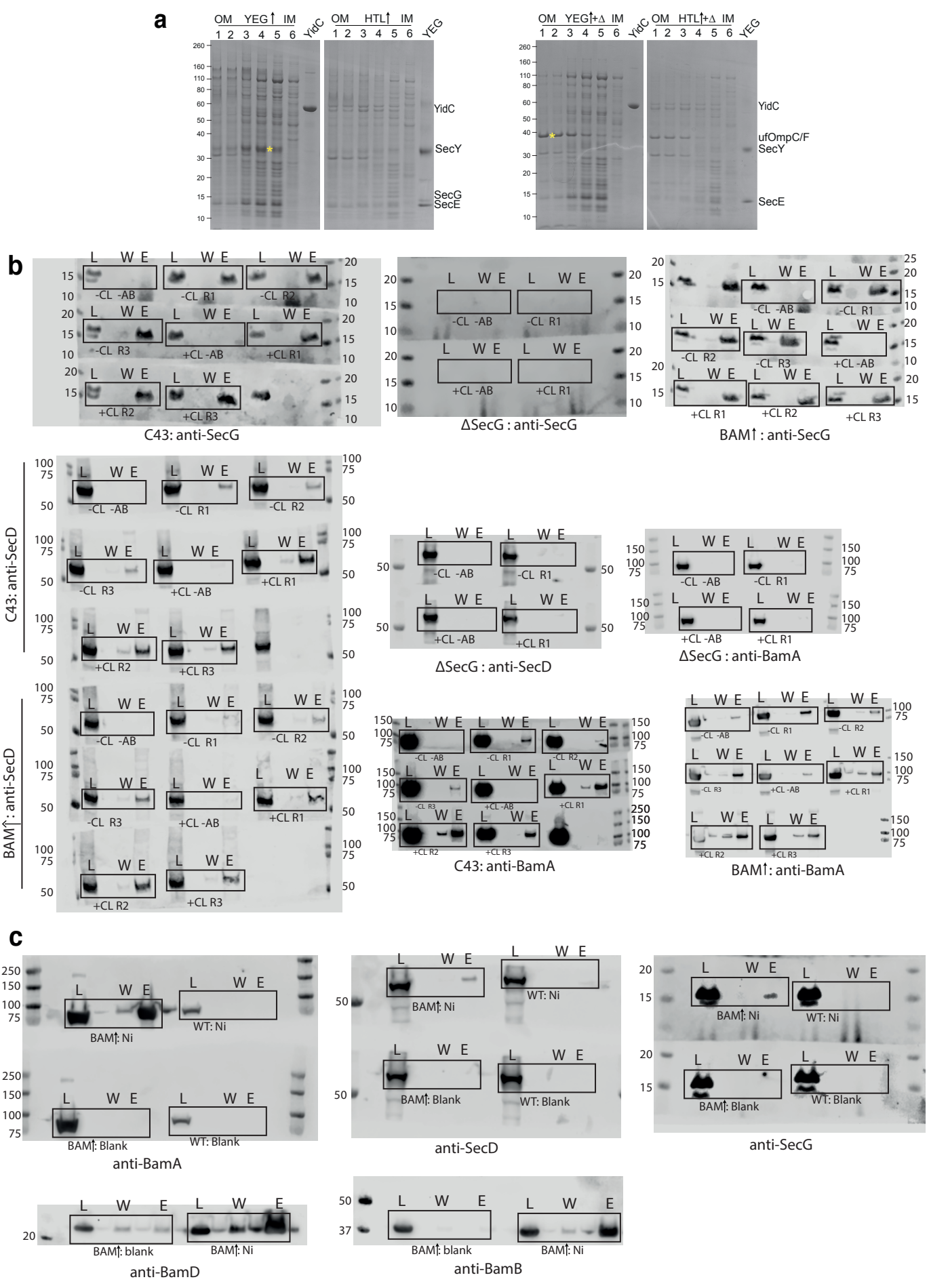
a
OM YEG↑ IM
1 2 3 4 5 6 YidC
OM HTL↑ IM
1 2 3 4 5 6 YEG
YidC
SecY
SecG
SecE
OM YEG↑+Δ IM
1 2 3 4 5 6 YidC
OM HTL↑+Δ IM
1 2 3 4 5 6 YEG
YidC
ufOmpC/F
SecY
SecE
b
L W E
-CL -AB
-CL R1
-CL R2
-CL R3
+CL -AB
+CL R1
+CL R2
+CL R3
C43: anti-SecG
ΔSecG : anti-SecG
BAM↑ : anti-SecG
C43: anti-SecD
BAM↑: anti-SecD
ΔSecG : anti-SecD
ΔSecG : anti-BamA
C43: anti-BamA
BAM↑: anti-BamA
c
BAM↕: Ni
WT: Ni
BAM↕: Blank
WT: Blank
anti-BamA
anti-SecD
anti-SecG
BAM↕: blank
BAM↕: Ni
anti-BamD
BAM↕: blank
BAM↕: Ni
anti-BamB

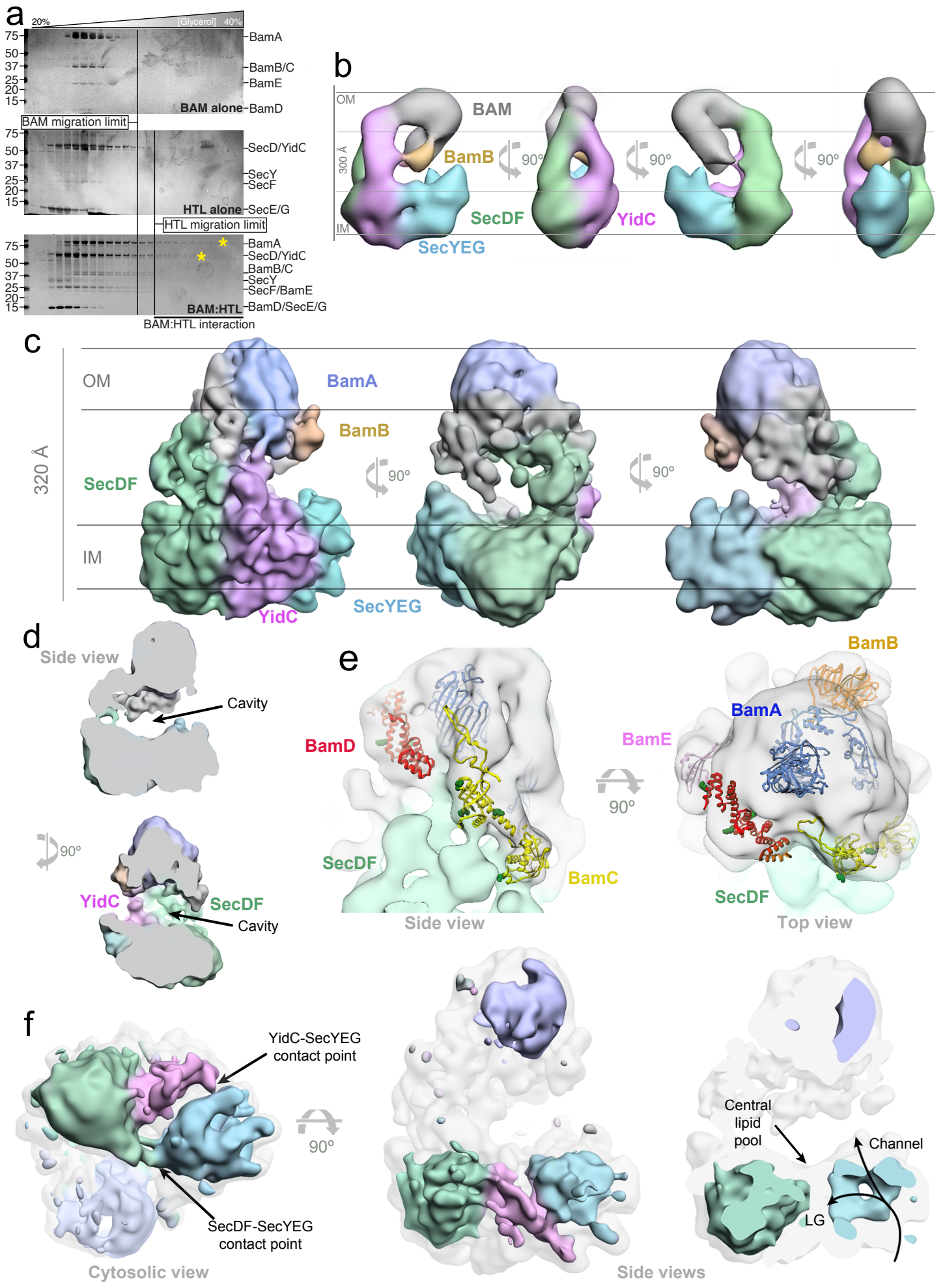
a
20%
[Glycerol]
40%
75
50
37
25
20
15
BamA
BamB/C
BamE
BAM alone
BamD
BAM migration limit
SecD/YidC
SecY
SecF
HTL alone
SecE/G
HTL migration limit
BamA
SecD/YidC
BamB/C
SecY
SecF/BamE
BAM:HTL
BamD/SecE/G
BAM:HTL interaction
b
OM
BAM
300 Å
BamB
90°
SecDF
YidC
IM
SecYEG
c
OM
BamA
BamB
320 Å
SecDF
90°
IM
YidC
SecYEG
d
Side view
Cavity
90°
YidC
SecDF
Cavity
e
BamD
SecDF
BamC
Side view
90°
BamB
BamA
BamE
SecDF
Top view
f
YidC-SecYEG
contact point
90°
SecDF-SecYEG
contact point
Cytosolic view
Central
lipid
pool
Channel
LG
Side views

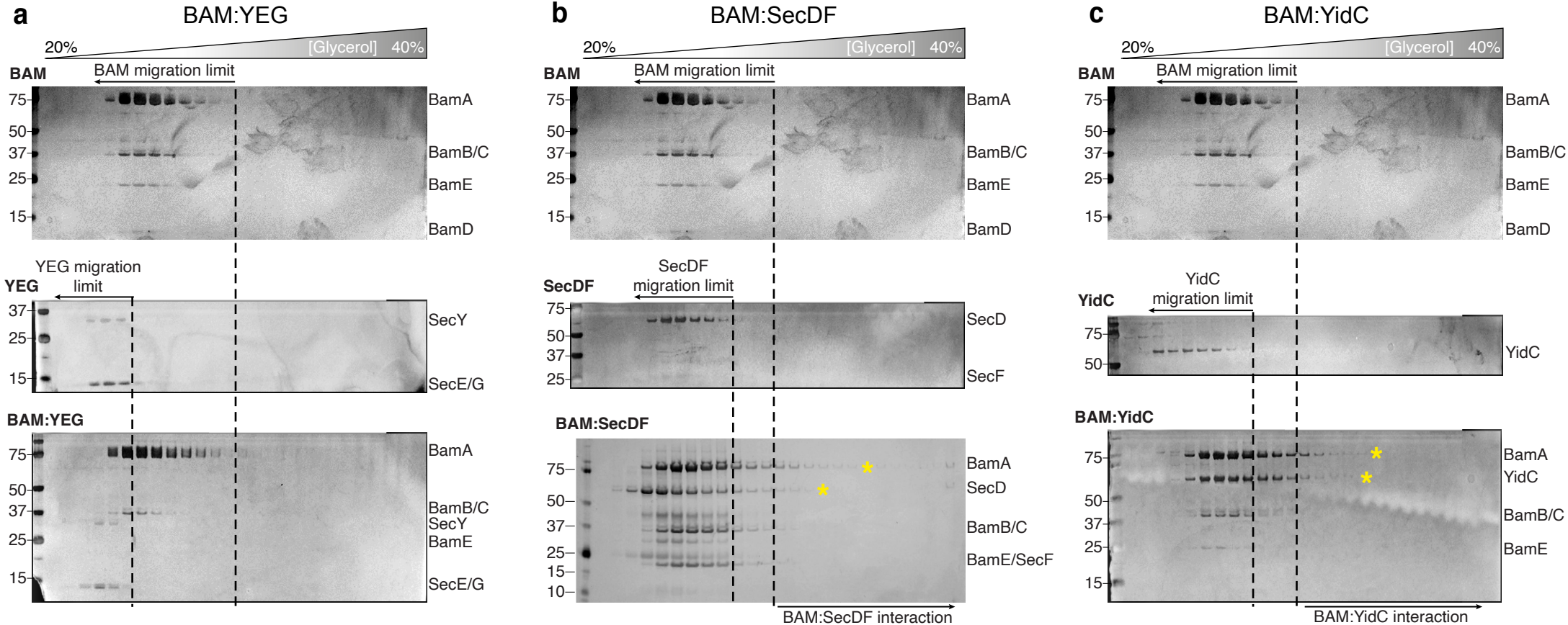
a
BAM:YEG
20%
[Glycerol]
40%
BAM
BAM migration limit
75
50
37
25
15
BamA
BamB/C
BamE
BamD
YEG migration limit
YEG
37
25
15
SecY
SecE/G
BAM:YEG
75
50
37
25
15
BamA
BamB/C
SecY
BamE
SecE/G
b
BAM:SecDF
20%
[Glycerol]
40%
BAM
BAM migration limit
75
50
37
25
15
BamA
BamB/C
BamE
BamD
SecDF
SecDF migration limit
75
50
37
25
SecD
SecF
BAM:SecDF
75
50
37
25
15
10
BamA
SecD
BamB/C
BamE/SecF
BAM:SecDF interaction
c
BAM:YidC
20%
[Glycerol]
40%
BAM
BAM migration limit
75
50
37
25
15
BamA
BamB/C
BamE
BamD
YidC
YidC migration limit
75
50
YidC
BAM:YidC
75
50
37
25
15
BamA
YidC
BamB/C
BamE
BAM:YidC interaction

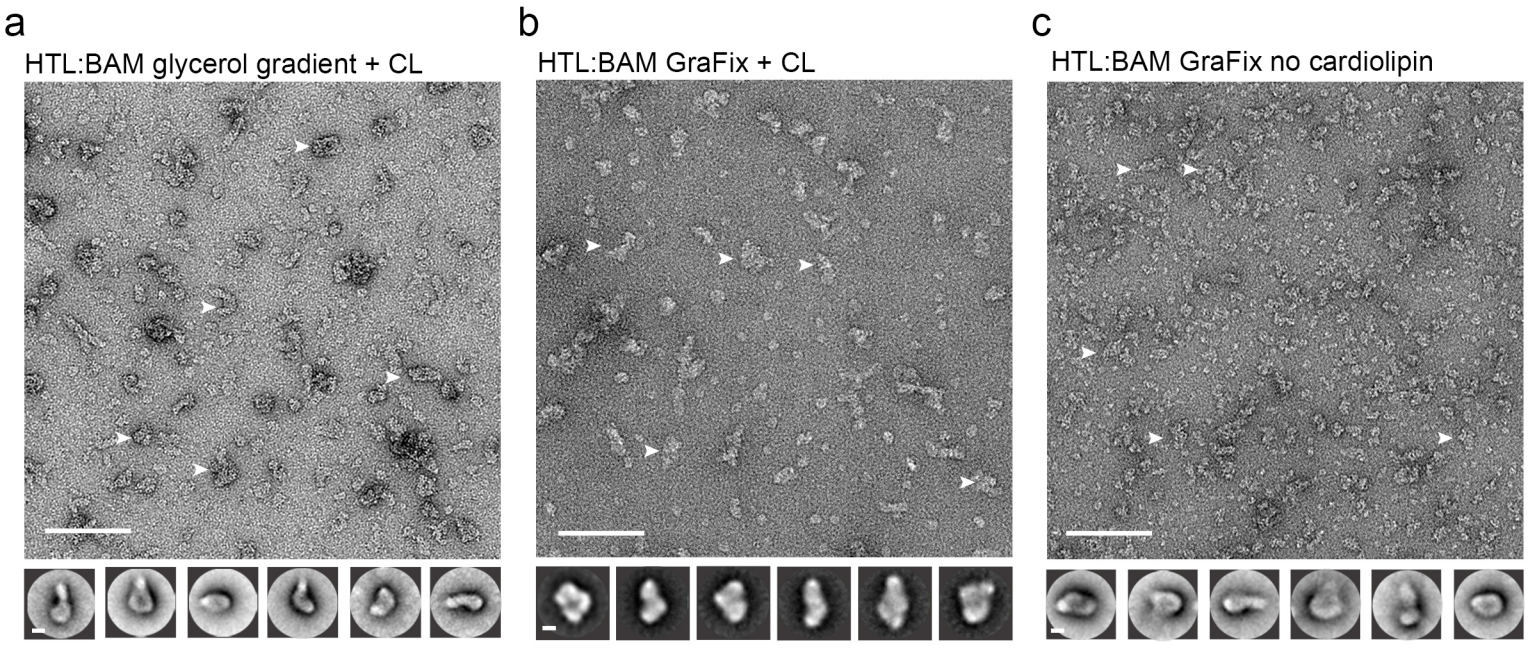
a
HTL:BAM glycerol gradient + CL
b
HTL:BAM GraFix + CL
c
HTL:BAM GraFix no cardiolipin

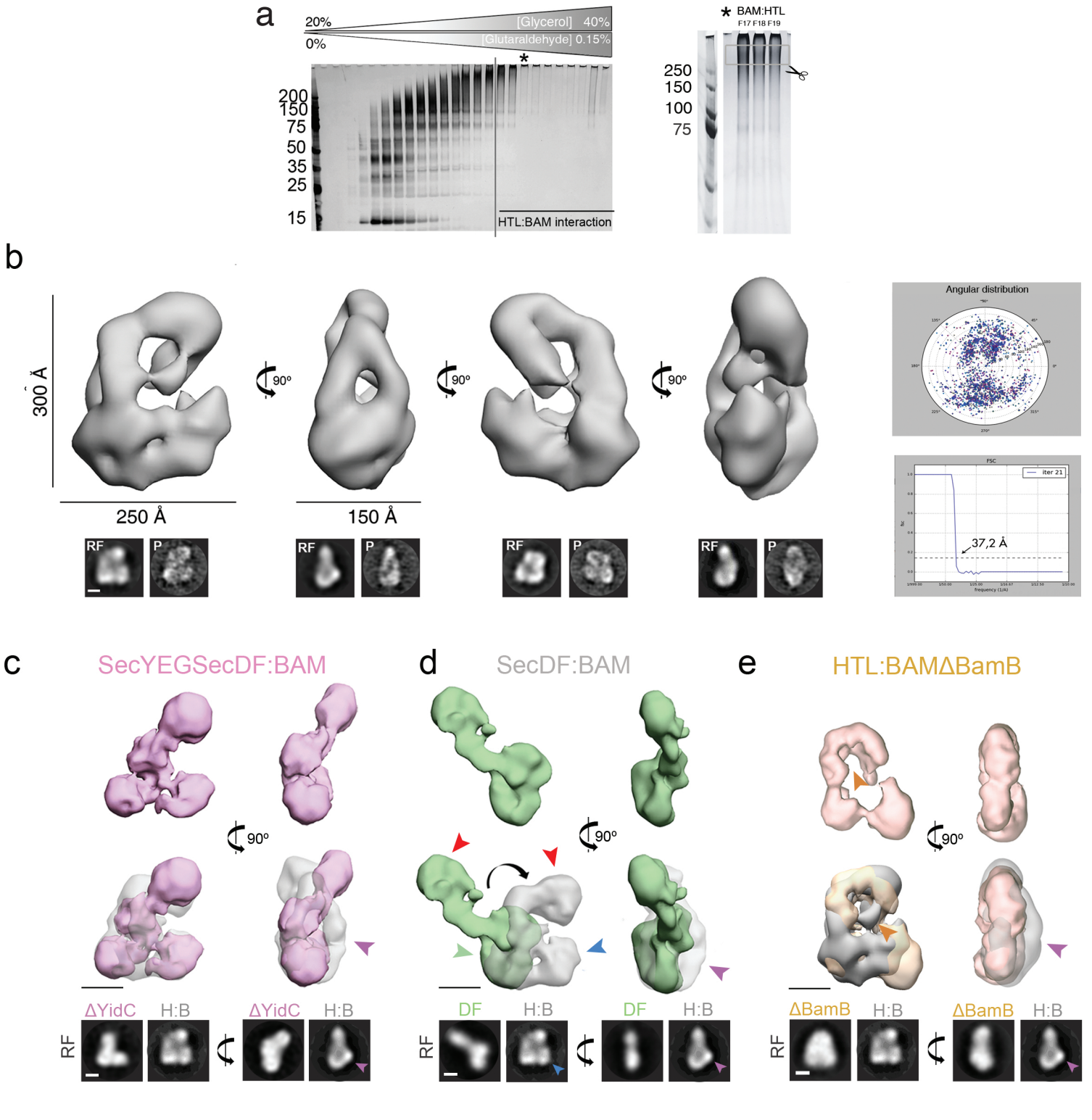
a
20%
0%
[Glycerol] 40%
[Glutaraldehyde] 0.15%
*
200
150
75
50
35
25
15
HTL:BAM interaction
* BAM:HTL
F17 F18 F19
250
150
100
75
b
300 Å
90°
250 Å
150 Å
RF
P
Angular distribution
FSC
iter 21
37,2 Å
frequency (1/Å)
c
SecYEGSecDF:BAM
ΔYidC
H:B
d
SecDF:BAM
DF
e
HTL:BAMΔBamB
ΔBamB

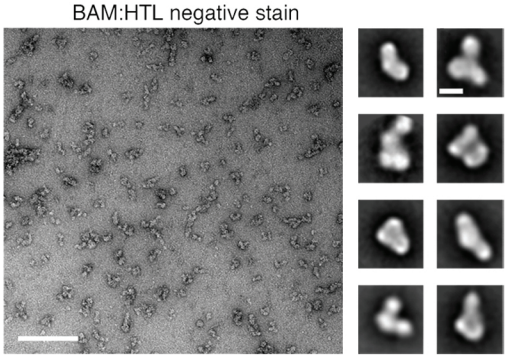

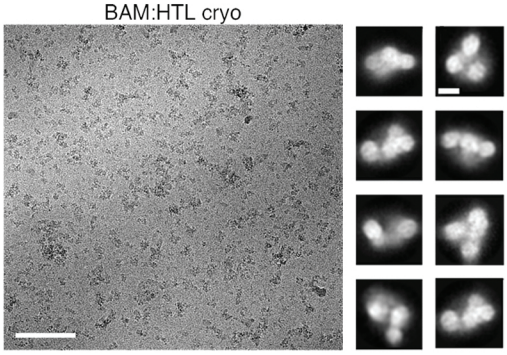

Set I

357,347 particles

↓ 2x 2D classif.

293,541 particles

Set II

482,498 particles

↓ 2x 2D classif.

314,952 particles

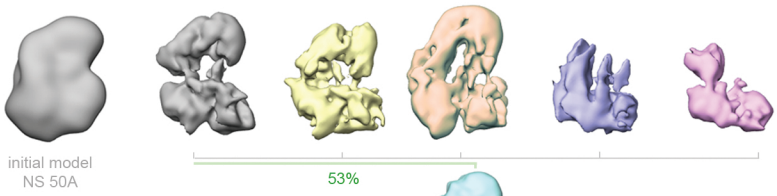

3x 3D classif.

3D auto-refine
97,553 particles

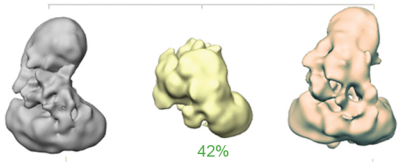

Projection Matching
41,652 particles

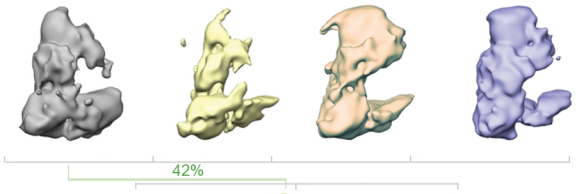

3x 3D classif.

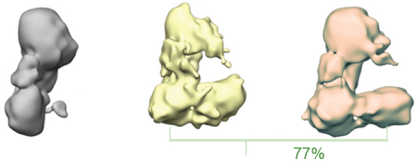

3D auto-refine
55,147 particles

96,799 particles

reference model

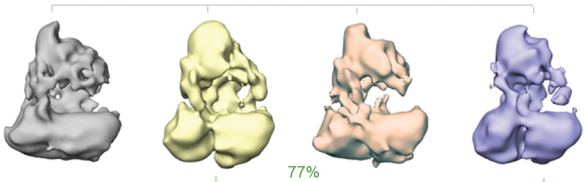

2x 3D classif.

3D auto-refine
74,222 particles

Cylindrical mask

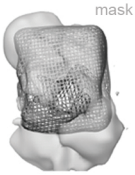

back view

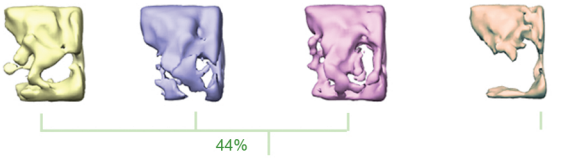

3D auto-refine
29,245 particles

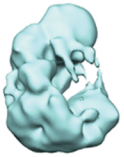

3x 3D classif.

Top mask

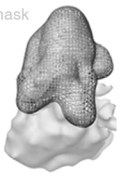

lateral view 1

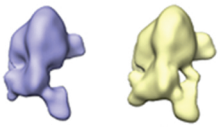

lateral view 2

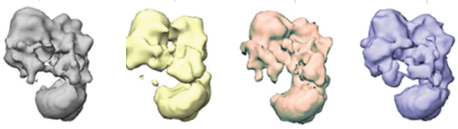

2x 3D classif (no mask)

12,779 particles

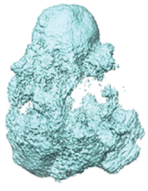

3D auto-refine
27 Å

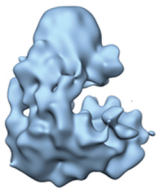

Post-processing
27 Å

3D classification

8,448 particles

Projection Matching

3D auto-refine
16,86 Å

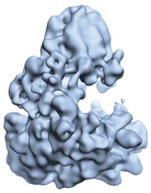

Post-procesing
18,23 Å

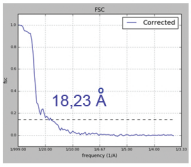

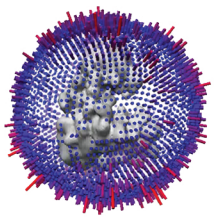

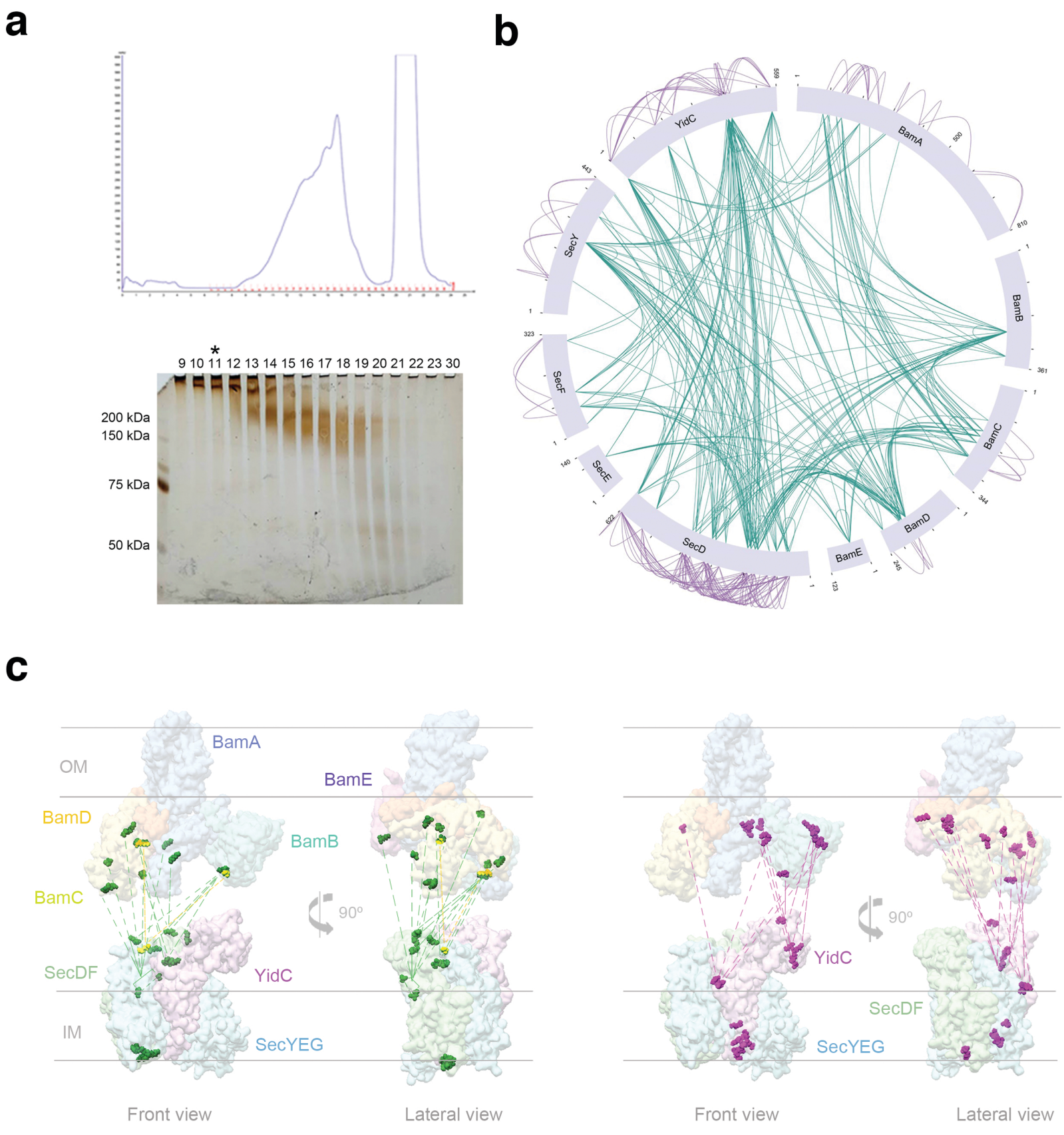
a
*
9 10 11 12 13 14 15 16 17 18 19 20 21 22 23 30
200 kDa
150 kDa
75 kDa
50 kDa
b
YidC
BamA
SecY
BamB
SecF
BamC
SecE
BamD
SecD
BamE
c
BamA
OM
BamE
BamD
BamB
BamC
90°
SecDF
YidC
IM
SecYEG
Front view
Lateral view
YidC
90°
SecDF
SecYEG
Front view
Lateral view

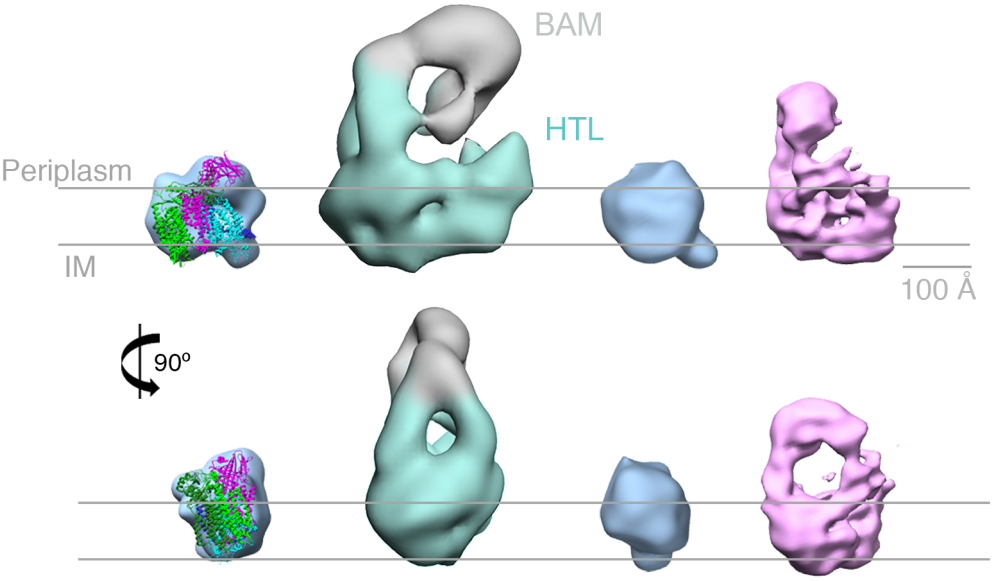
BAM
HTL
Periplasm
IM
100 Å
90º
CryoEM
HTL compact
(emd3506)
(i)
NS-EM
HTL:BAM
(ii)
NS-EM
HTL
compact
(iii)
NS-EM
HTL
open
(iv)

HTL-DDM - CL

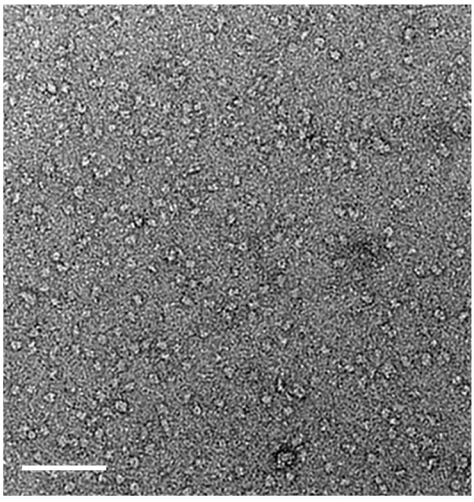

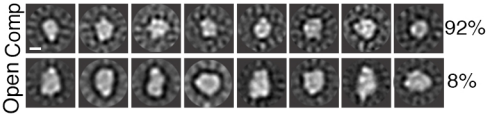

HTL-DDM + CL

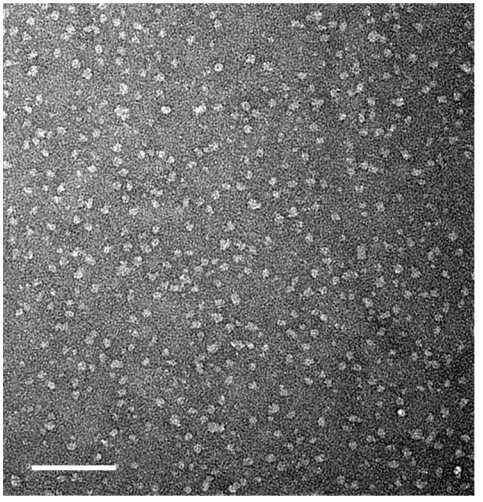

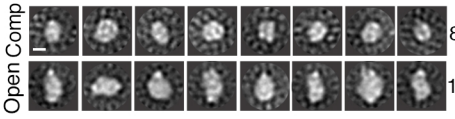

HTL-DDM glycerol gradient + CL

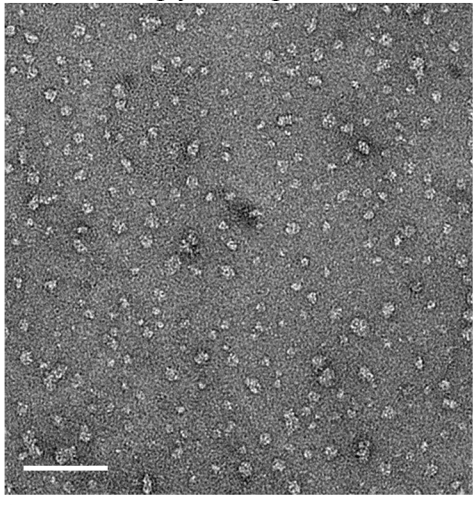

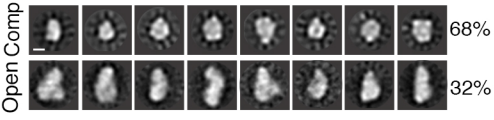

HTL-DDM GraFix + CL

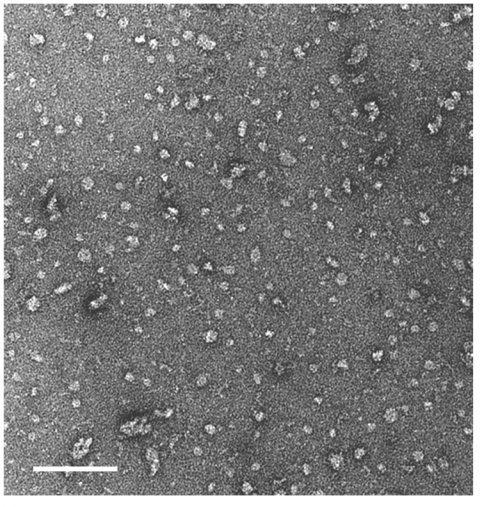

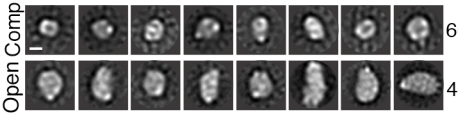

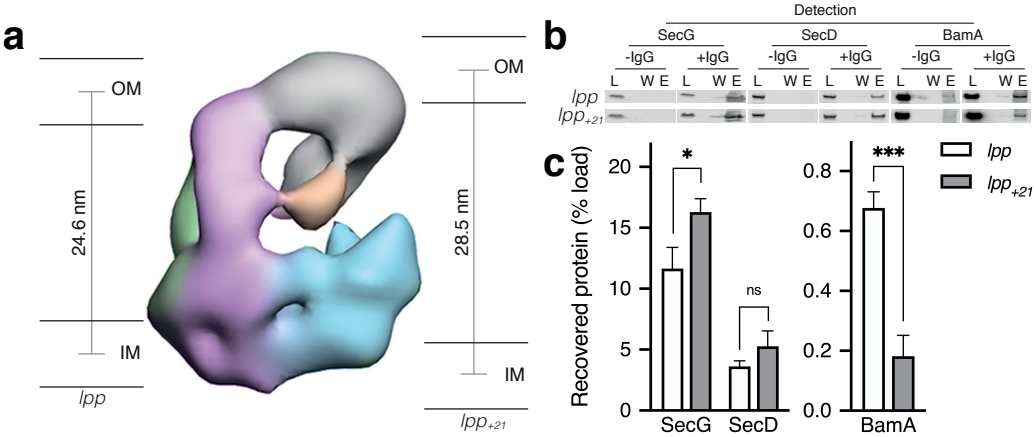
a
OM
24.6 nm
IM
lpp
OM
28.5 nm
IM
lpp+21
b
Detection
SecG
SecD
BamA
-IgG
+IgG
L W E
lpp
lpp+21
c
Recovered protein (% load)
lpp
lpp+21
*
ns
***
SecG
SecD
BamA

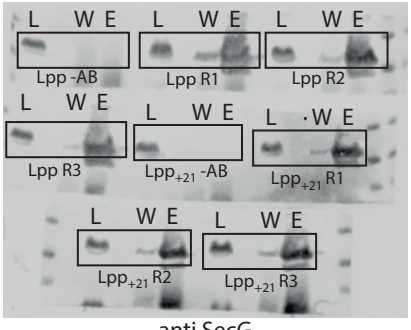

anti SecG

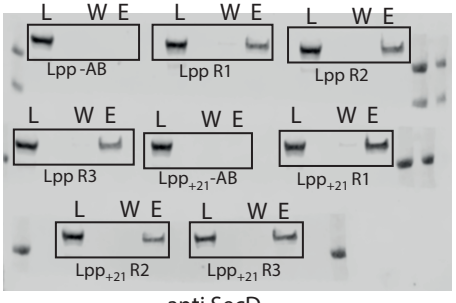

anti SecD

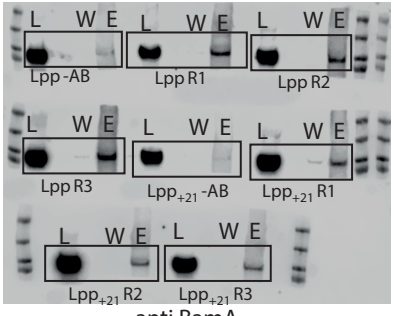

anti BamA

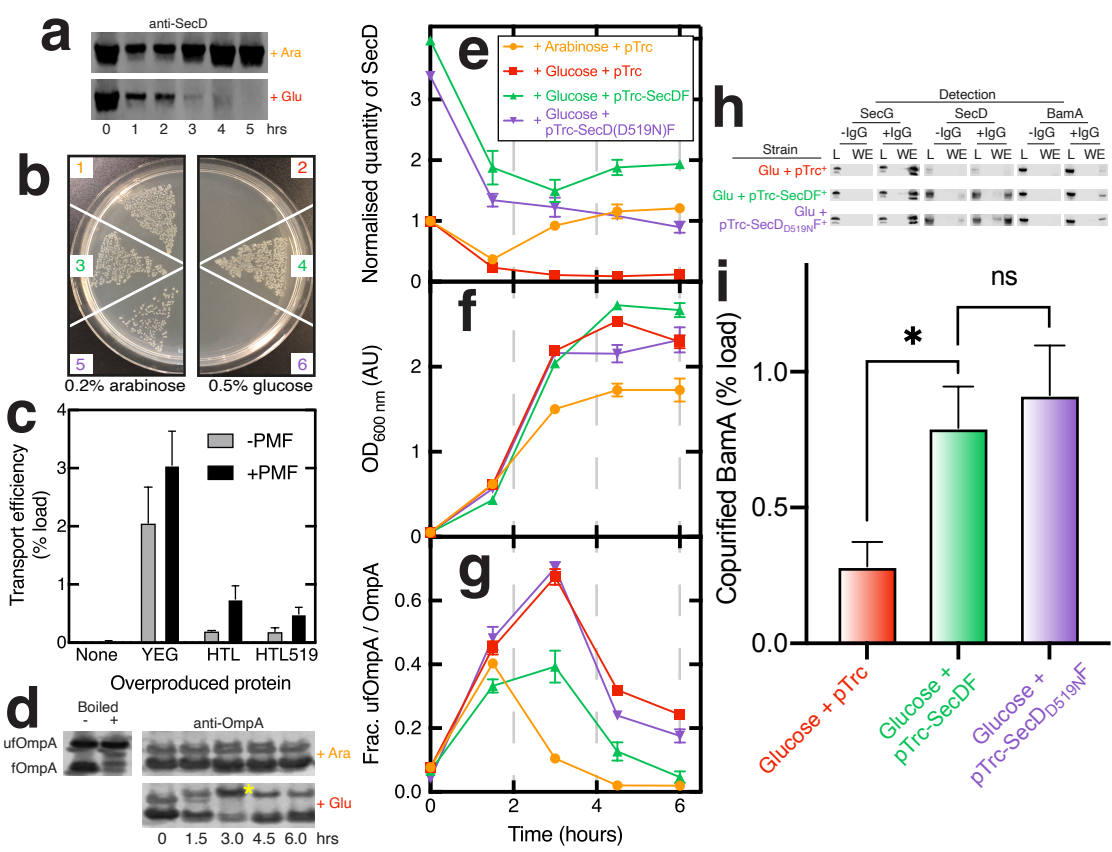
a
anti-SecD
+ Ara
+ Glu
0 1 2 3 4 5 hrs
b
1
2
3
4
5
6
0.2% arabinose
0.5% glucose
c
Transport efficiency (% load)
-PMF
+PMF
None
YEG
HTL
HTL519
Overproduced protein
d
Boiled
- +
ufOmpA
fOmpA
anti-OmpA
+ Ara
+ Glu
0 1.5 3.0 4.5 6.0 hrs
e
+ Arabinose + pTrc
+ Glucose + pTrc
+ Glucose + pTrc-SecDF
+ Glucose + pTrc-SecD(D519N)F
Normalised quantity of SecD
f
OD600 nm (AU)
g
Frac. ufOmpA / OmpA
Time (hours)
h
Detection
SecG
SecD
BamA
-IgG +IgG -IgG +IgG -IgG +IgG
Strain
L WE L WE L WE L WE L WE L WE
Glu + pTrc+
Glu + pTrc-SecDF+
Glu + pTrc-SecD D519N F+
i
Copurified BamA (% load)
ns
*
Glucose + pTrc
Glucose + pTrc-SecDF
Glucose + pTrc-SecD D519N F

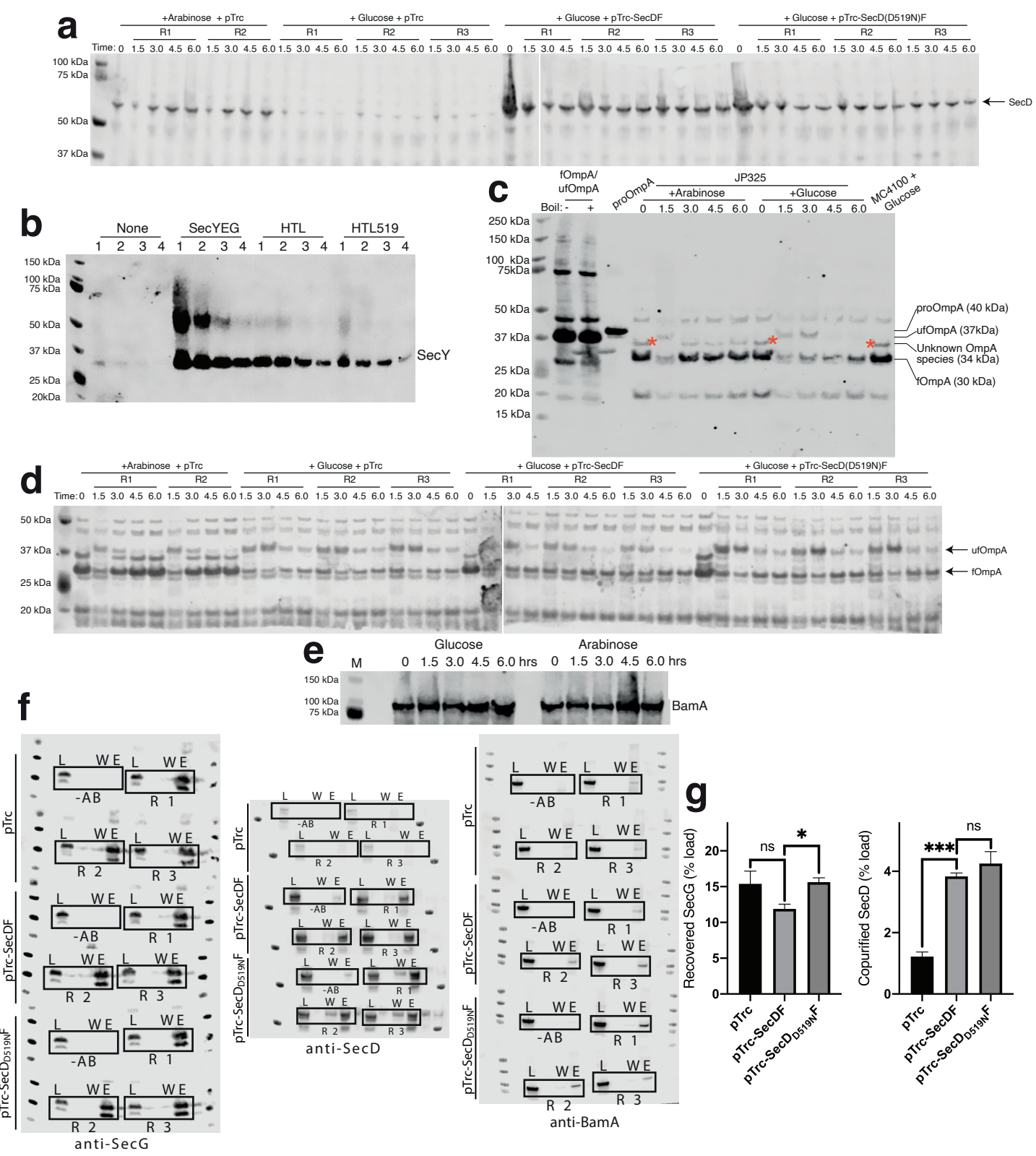
a
+Arabinose + pTrc
+ Glucose + pTrc
+ Glucose + pTrc-SecDF
+ Glucose + pTrc-SecD(D519N)F
R1
R2
R3
Time: 0 1.5 3.0 4.5 6.0
100 kDa
75 kDa
50 kDa
37 kDa
SecD
b
None
SecYEG
HTL
HTL519
1 2 3 4
150 kDa
100 kDa
75 kDa
50 kDa
37 kDa
25 kDa
20kDa
SecY
c
fOmpA/
ufOmpA
Boil: - +
proOmpA
JP325
+Arabinose
+Glucose
MC4100 + Glucose
0 1.5 3.0 4.5 6.0
250 kDa
150 kDa
100 kDa
75kDa
50 kDa
37 kDa
25 kDa
20 kDa
15 kDa
proOmpA (40 kDa)
ufOmpA (37kDa)
Unknown OmpA species (34 kDa)
fOmpA (30 kDa)
d
+Arabinose + pTrc
+ Glucose + pTrc
+ Glucose + pTrc-SecDF
+ Glucose + pTrc-SecD(D519N)F
R1
R2
R3
Time: 0 1.5 3.0 4.5 6.0
50 kDa
37 kDa
25 kDa
20 kDa
ufOmpA
fOmpA
e
Glucose
Arabinose
M
0 1.5 3.0 4.5 6.0 hrs
150 kDa
100 kDa
75 kDa
BamA
f
pTrc
pTrc-SecDF
pTrc-SecD$_{D519N}$F
L WE
-AB
R 1
R 2
R 3
anti-SecG
anti-SecD
anti-BamA
g
Recovered SecG (% load)
ns
*
Copurified SecD (% load)
***
ns
pTrc
pTrc-SecDF
pTrc-SecD$_{D519N}$F

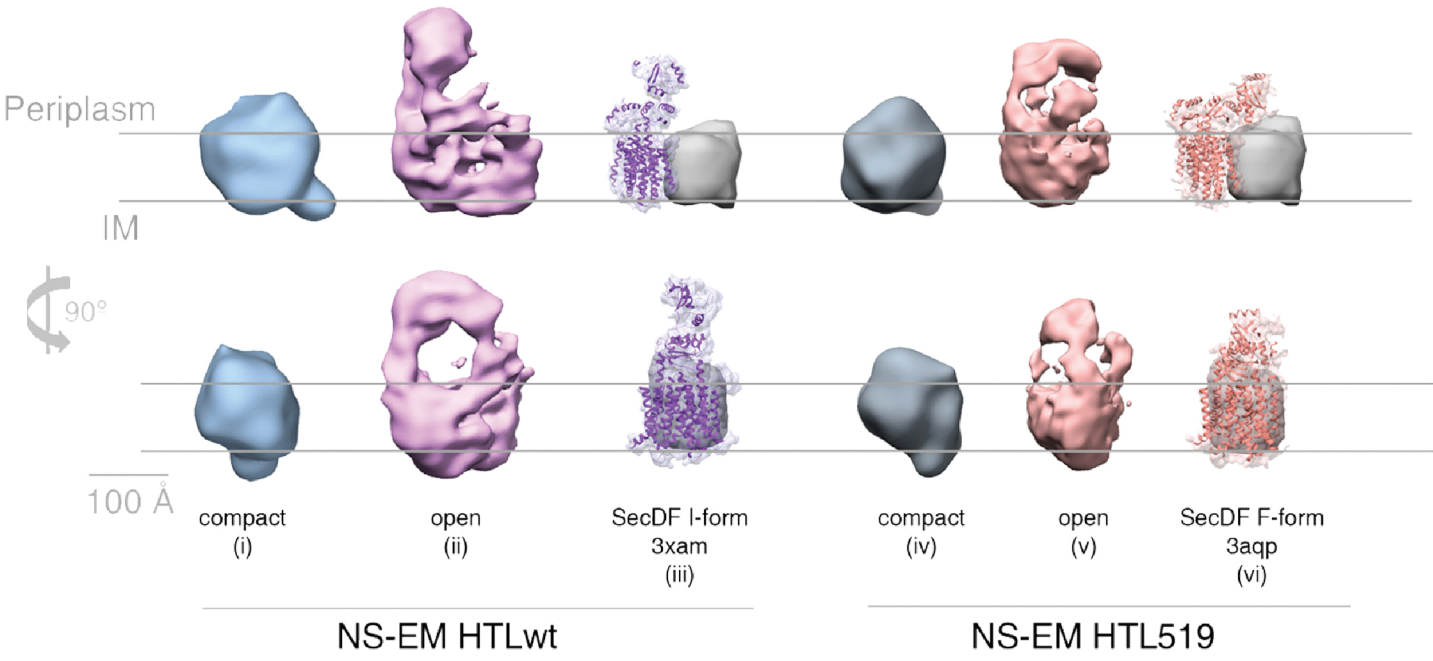
Periplasm
IM
90°
100 Å
compact
(i)
open
(ii)
SecDF I-form
3xam
(iii)
compact
(iv)
open
(v)
SecDF F-form
3aqp
(vi)
NS-EM HTLwt
NS-EM HTL519

HTL-DDM + CL

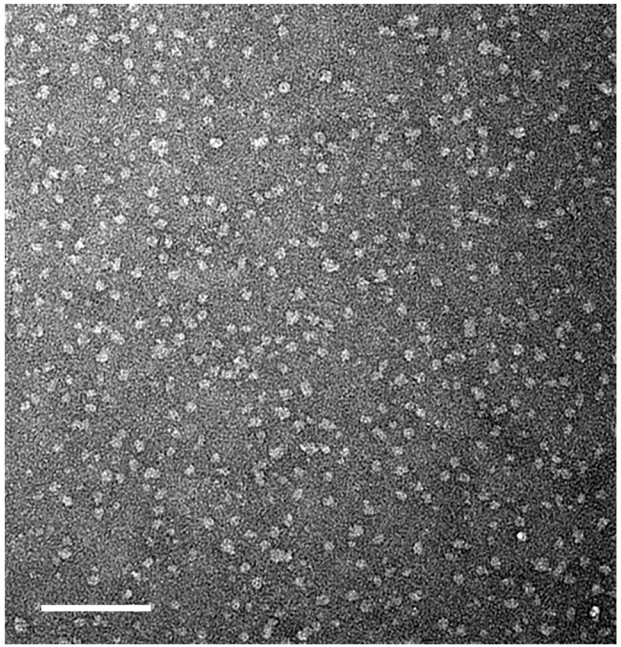

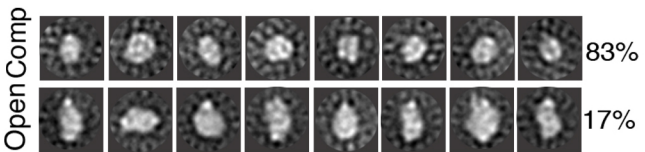

HTL519-DDM + CL

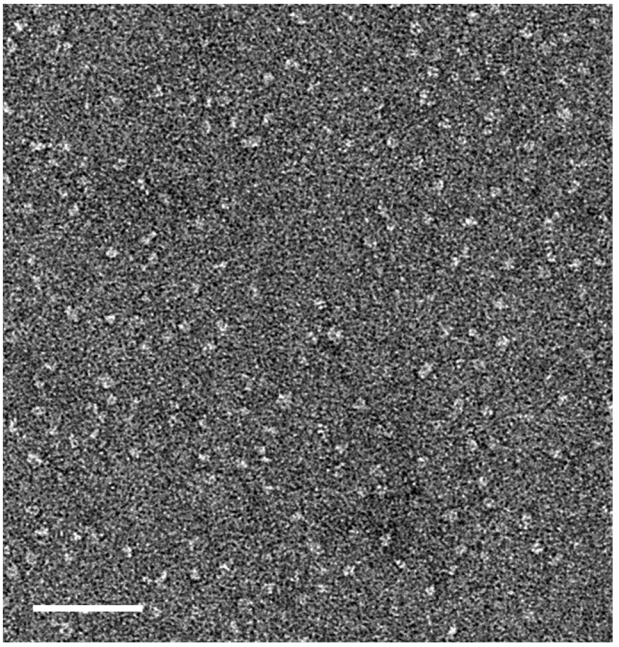

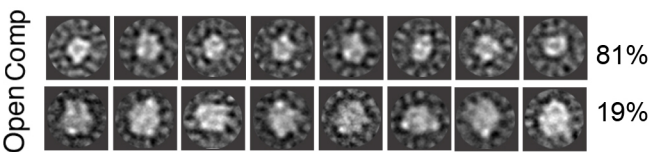

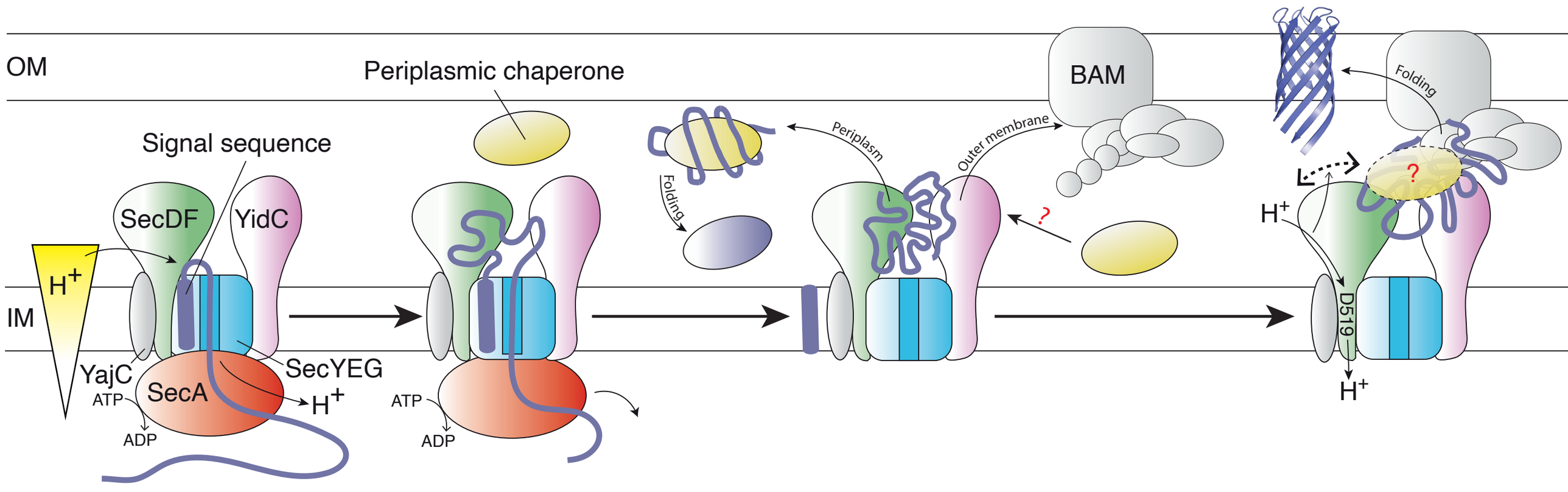
OM
IM
Periplasmic chaperone
Signal sequence
SecDF
YidC
H+
YajC
SecA
SecYEG
ATP
ADP
H+
ATP
ADP
Folding
Periplasm
Outer membrane
BAM
?
Folding
?
H+
D519
H+